JOURNAL
of the
OPTICAL SOCIETY
OF AMERICA

VOLUME 22
No. 5

MAY
1932

AN ECLIPSE PROJECTOR FOR THE FRANKLIN INSTITUTE MUSEUM

By James Stokley

[The Franklin Institute, Philadelphia, Penna.
Received January 30, 1932]

So striking an event is a total eclipse of the sun that it is not surprising that many attempts have been made to reproduce its effects artificially. The famous orrery, made about 1769 by David Rittenhouse in Philadelphia, had one section to show the time, duration, and place of visibility of both solar and lunar elipses during a 10,000 year period, centered at the time that it was built. This orrery, which has been in the possession of the University of Pennsylvania since its construction, has been loaned to The Franklin Institute, for exhibition in its new Museum. It is now being restored to the condition in which Rittenhouse left it, thus completing the work begun a few years ago by Prof. Maurice J. Babb, when the eclipse mechanism was placed in operation.

Rittenhouse, however, made no effort to simulate an eclipse as seen in the sky, with the gradual covering of the solar disc by the Moon and the sudden appearance of the corona. In 1869, this was done by Joseph Zentmayer, a well-known Philadelphia optician, and his apparatus, which is very simple, is now in the possession of the Franklin Institute. It is shown in Fig. 1, and consists of three parts. First is a glass transparency prepared photographically from a drawing, showing the Sun, with spots, prominences (colored red) and the corona. Over this, and

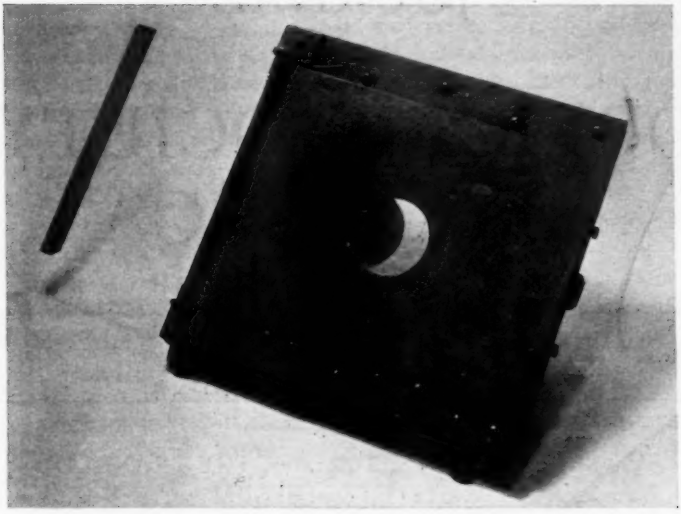

FIG. 1A. *Zentmayer eclipse slide showing partial phase well advanced.*

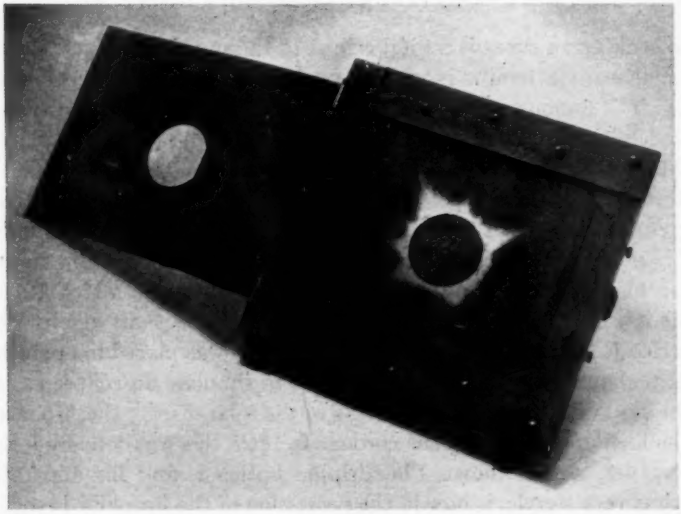

FIG. 1B. *Zentmayer eclipse slide showing total phase. The sliding glass holding the "Moon," has completely obscured the hole representing the Sun and has released the cover, thus exposing the corona.*

hinged at one side, is a thin metal cover, with a circular hole in the center, the same diameter as the solar disc. The hinge is provided with a spring, to lift it, and a catch, at the opposite end, holds it down. Sliding in grooves in the frame to which the transparency is attached is a rectangular piece of glass, to which is cemented a metal disc, slightly larger than the hole in the metal cover. This disc, which represents the Moon, slides into a position in which the Sun image, the disc and the hole are concentric.

The apparatus is used in a stereopticon, from which the bellows must be removed in order to allow sufficient clearance to the metal cover when it lifts. When first displayed, the cover is down, and the sliding

FIG. 2. *Franklin Institute eclipse projector as constructed by the Bausch and Lomb Optical Company. The large glass disc, carrying the smaller Moon discs, rotates in a counter clock-wise direction. The stereopticon on the left projects the Baily's bead, the one on the right, the corona.*

glass is withdrawn sufficiently that the complete solar disc is seen. By hand, the slide is slowly pushed inward, and the Moon begins to encroach on the Sun, as seen on the screen. Finally only the narrow crescent remains, and then, just as the Sun is completely covered, the forward end of the glass slide releases the catch holding down the cover. The spring lifts the cover very suddenly, and on the screen is seen the dark lunar disc, surrounded by the corona, and prominences. This completes the demonstration, as no provision is made for showing third and fourth contacts.

Essentially, the new instrument, as constructed by the Bausch and Lomb Optical Company, in 1931, is a triple stereopticon, as shown in

Fig. 2. The center lantern projects a circular spot of light representing the Sun, by means of a metal slide in which is cut a hole 31 mm in diameter. Revolving in front of this is a glass disc, 254 mm in diameter, near the edge of which is attached a series of six smaller occulting discs of black bakelite. One occulting disc is slightly larger than the hole representing the Sun, but displaced so as partially to cover the hole, as it passes in front. It leaves a narrow crescent of light which slips around from one limb to the other, thus simulating a partial eclipse. The next disc is slightly smaller than the hole, but passes across the center of it, thus producing the effect of an annular eclipse. The third

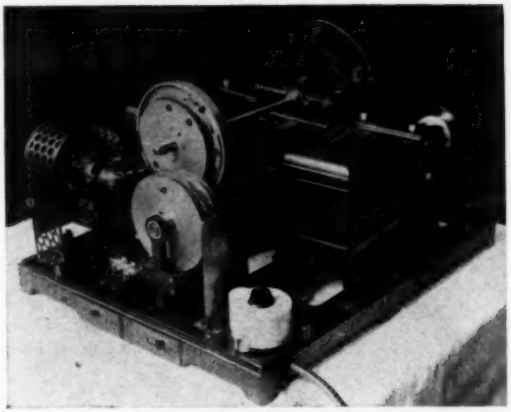

FIG. 3. *Franklin Institute eclipse projector from the rear, showing the driving motor, gears, cams to operate the mercury switches, and automatic dissolves, and controller.*

disc is the same size as for the partial eclipse, and passes centrally across the hole, to produce the total eclipse effect. The other three occulting discs duplicate those mentioned, six being used in order to make the glass disc fairly large. In this way the occulting discs pass across the hole almost laterally.

Just as "totality" is approached, and the narrow crescent of "sunlight" disappears, two mercury switches, operated by cams, connect the other two lanterns. At this point, the one on the right is covered by an iris diaphragm in front of the lens, while the one on the left shines on the screen. The slide in this lantern consists of a sheet of metal in which is drilled a circular row of small holes. These appear on the screen as a series of bright spots, in the same position as the last visible crescent, simulating the Baily's beads.

About a second after the "Baily's beads" appear on the screen, an-

other cam operates the two diaphragms, the left lantern being quickly covered, and the right one suddenly opened, projecting a picture of the eclipsed Sun, with the corona and prominences, the latter colored red.

The "total eclipse" lasts about ten seconds, then the iris dissolve is again operated, by means of the cam, extinguishing the "corona" and showing once more the "Baily's beads", this time on the opposite limb of the "Sun". The mercury switches are then opened, the "beads" quickly disappear, and a narrow crescent reappears, as the hole is gradually uncovered by the motion of the glass disc. Fig. 3, of the machine from the rear, shows the gearing, cams, and mercury switches.

In order to show the motions clearly, the apparatus operates at such a speed that each eclipse takes about a minute, from first to last contacts. This introduced a difficulty, because "totality", similarly speeded, would last only a fraction of a second, and it was desired to have it long enough for the visitor to observe the details. The glass disc, therefore, is retarded, while the "corona" appears, for about 10 seconds. This is accomplished without any jerkiness being perceptible on the screen.

Two other features of the machine deserve specific mention. One is a shutter, actuated by another cam, that operates in front of the Baily's beads slide. The holes representing the beads form a complete circle, but they must only appear on one limb at a time. This shutter covers one half of the circle at the beginning and the other half at the end of "totality". It was also desired that the name of each kind of eclipse, partial, annular or total, should appear on the screen before it begins. This is accomplished by a slide showing the three names, and placed above the hole representing the Sun. A smaller opaque disc attached to, and concentric with, the large glass disc, revolves in front of the name slide. A series of slits is arranged in this disc in such a way that the proper name is exposed at the right time, and a cam-actuated shutter exposes it for a few seconds just before each first contact.

As it is intended that the apparatus should be concealed, and the effects shown on a translucent screen, the direction of rotation of the disc is adjusted accordingly. The lanterns are of standard type, with the usual lamphouses, condensers and projection lenses, but no bellows are provided. The two outer lanterns can be moved laterally, in order to register the images of the Sun, Baily's beads and corona on screens at varying distances. The carriers of the slides for the Baily's beads, and the corona, are furnished with vertical and lateral movements for a fine adjustment. Five hundred watt lamps are used for each lantern. Even though only the center lantern is turned on all the time, considerable heat is generated. The entire apparatus, which is covered with a sheet

metal hood, is well ventilated, and a fan attached to the motor produces a continual current of air through its interior. Fig. 4 shows the machine in use, with the corona visible. The principal stages in the

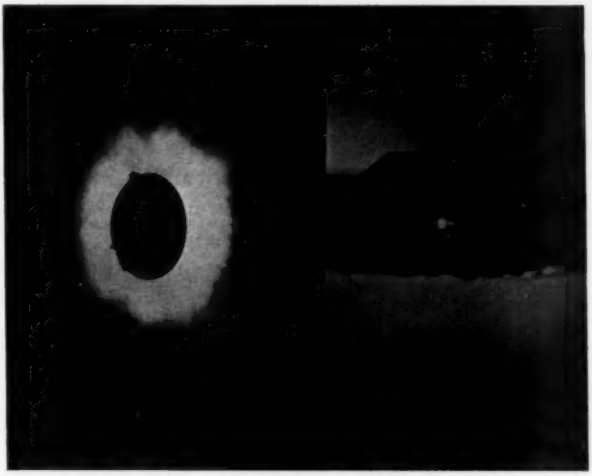

FIG. 4. *Franklin Institute eclipse projector in use, showing the corona projected on the screen.*

total eclipse series are shown in Fig. 5, reproducing a set of photographs made directly from the screen.

In conclusion, the writer desires to express his gratitude to the officials of the Bausch and Lomb Optical Company for their cordial cooperation in solving so competently a rather unusual problem. Mr. G.

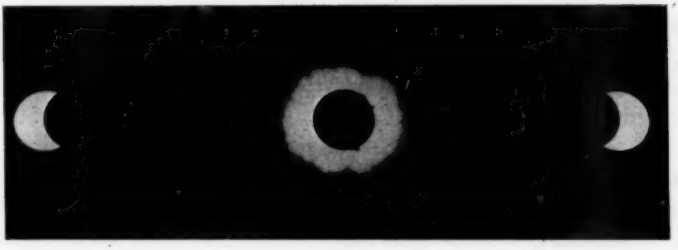

FIG. 5. *Five stages in the total eclipse series, photographed directly from the screen.*

Gallasch, of the company's engineering section, and director of their observatory, and Mr. E. H. Anthes, of the New York office, are particularly deserving of thanks.

ON THE CONCAVE GRATING SPECTROGRAPH, ESPECIALLY AT LARGE ANGLES OF INCIDENCE

By J. E. Mack,* J. R. Stehn,* and Bengt Edlén¶

[Department of Physics, University of Wisconsin, and Physics Laboratory, University, Uppsala, Received November 9, 1931]

ABSTRACT

On the physical optics of the perfect concave grating. An extension of the theory of the concave grating to the fourth order approximation shows that the diffraction pattern for a spectral line is different in shape from that for a plane grating. A generalization of Rayleigh's definition of resolving power allows the computation of the resolving power of a grating in terms of an "effective width"; i.e., the width of a plane grating having the same resolving power as the concave one in question. At grazing incidence (a case of particular interest in the spectroscopy of the extreme ultraviolet) this effective width is of the order of 1 cm.

Optimum width of the grating. The optimum width of a grating (for resolving power and intensity), as a function of wave length and angle of incidence, is found. A table of values of this width shows that, in cases of large angles of incidence and short wave lengths, the gratings ordinarily used in the past have been considerably wider than the optimum.

Elimination of grazing incidence ghosts. Experiments show that the reduction of the width of a grating to about the optimum eliminates the ghosts (different from Rowland ghosts) which occur in the neighborhood of strong lines in grazing incidence spectrograms.

Economies in ruled area. In many cases the lengths of the rulings and of the spectrograph slit, as well as the number of rulings, may be smaller than is now customary.

Inexactness of the grating condition equation. Though the intensity pattern really depends upon the value of

$$\left|\int_{-H}^{+H} f(\eta) e^{i(\alpha\eta+\eta^4+\gamma\eta^5+\cdots)} d\eta\right|^2,$$

usually the approximations $f(\eta)=$ a constant, and γ etc. $=0$ are made. With the complete expression, the ordinary grating condition equation, $\sin\theta+\sin\theta'=m\lambda/\sigma$, becomes inexact. The error is below the threshold of importance for ordinary measurements.

The spectrograph. The questions of symmetric adjustment of the grating about the point of tangency to the Rowland circle, non-uniform illumination of the grating, and finite slit width are considered. The theoretical resolving power agrees well with experimental values.

I. On the Physical Optics of the Perfect Concave Grating

When Rowland, Glazebrook, Rayleigh, Mascart, and others, about 1883, were perfecting the theory of the concave grating,[1] they realized that it is not theoretically such a simple instrument as the plane grating, but that there is a slight aberration, or difference in phase at the image, between the light from the outer edge of the grating and that

* Dept. of Physics, U. of Wisconsin.

¶ Physics Lab., U. Uppsala.

[1] For a complete history and bibliography, as well as the clearest (Runge's) general discussion of the theory of the concave grating, see Kayser, "Handbuch der Spektroskopie," vol. 1, pp. 450–482 (1900).

from the center. The main term in this aberration is proportional to the fourth power of the grating width. However, Rowland showed that the approximation is so close for the mountings then in vogue that the aberration would not be serious[2] except for gratings considerably wider (in the direction perpendicular to the rulings) than it has ever been practical to construct. Since that time it has been customary to treat concave gratings as though they were plane, insofar as their resolving power is concerned. The refinement of the theory of the resolving power of a concave grating beyond the first approximation was unnecessary until the recent developments in the experimental technique of extreme ultraviolet spectroscopy, which have culminated in the work of Professor

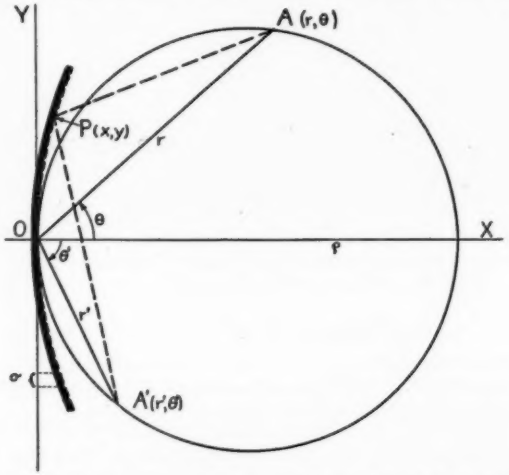

FIG. 1. *Section of grating spectrograph, perpendicular to direction of rulings. P is on the surface of the grating; A, O, A', on the Rowland circle. ρ = radius of grating = diameter of Rowland circle.*

Siegbahn and his students. The object of this section of the present investigation is to extend the resolving power theory to an accuracy sufficient for modern experimental needs (which involves a generalization of Rayleigh's definition of resolving power) as well as to give some idea of the useful size of gratings in actual cases.

Let us consider the grating as part of the spherical surface $x^2-2\rho x+y^2+z^2=0$, with the origin O at the center of the ruled portion of the grating (see Fig. 1). Rectangular coordinates are useful in this expres-

[2] That is, the discrepancy in path would be less than $\lambda/4$. The relationship between this criterion and the results of this investigation, is discussed in footnotes 8 and 12.

sion because the rulings are ordinarily made at the intersections of equidistant planes $y=n\sigma$ with the spherical surface. Here σ is the grating interval and n is an integer, $-N/2 \leqq n \leqq +N/2$, where N is the total number of lines in the grating. Except for the typical point $P(x, y, z)$ on the grating, we shall use cylindrical coordinates (r, θ, c).

The general problem would require that we know the phase at any point $A'(r', \theta', c')$ of light from any other point $A(r, \theta, c)$ scattered from a point $P(x, y, z)$ of the grating. For most practical purposes we may restrict ourselves, however, to the consideration of points A and A' on the cylinder

$$r = \rho \cos \theta$$

whose intersection with the xy plane is the Rowland circle.[3] In that case, it can be shown[4] that

$$\overline{AP}^2 = (\rho \cos \theta - y \sin \theta)^2 + \sin^2 \theta(z^2 + x^2) - 2cz + c^2 \qquad (1)$$

and the same expression, but with primed coordinates, holds for $\overline{PA'}^2$. Then the phase at A' is given by $2\pi/\lambda$ times the path, or by $2\pi/\lambda \cdot (\overline{AP}+\overline{PA'})$.

At present we are interested only in the resolving power, and need consider only the two dimensional problem $(c, c', z=0)$.[5] If we expand $\overline{AP}$ in powers of y,

$$\overline{AP} = (\rho \cos \theta - y \sin \theta)\sqrt{1 + \frac{x^2 \sin^2 \theta}{(\rho \cos \theta - y \sin \theta)^2}}$$

$$= \rho \cos \theta - y \sin \theta + \frac{y^4 \tan \theta \sin \theta}{8\rho^3} + \frac{y^5 \tan^2 \theta \sin \theta}{8\rho^4} + \cdots . \qquad (2)$$

Our accuracy is sufficient[6] if we include only terms up to y^4. The path is

[3] The practical extension into three dimensions is obviously the cylinder, for the photographic plate, cut from a plane, can not take a second curvature.

[4] By extending the method of Kayser, l.c., pp.456–458, to $c \neq 0$.

[5] By carrying the method of Section IV, which considers the three dimensional case, to a higher degree of accuracy, it can be shown that the light scattered from the whole length of one ruling has a resultant amplitude vector $\mathfrak{d}_n$ whose magnitude is practically independent of y (so long as $y << r$, the case in any ordinary grating) and has the same phase dependence on y as the light coming from the line $z=0$. This statement is true to a higher degree of approximation when $c, c'=0$ (small source near the slit, and central axis of photographic plate). Hence the simplification made here is justified.

[6] The term independent of y is dominant here, and the linear term is next in magnitude. But the resolving power will be seen in the equations below to depend upon the phase differences between the path $\overline{AP}+\overline{PA'}$ throughout the range of points P (i.e., of ordinates y). Since r is independent of y, $(r+r')$ can not be expected to contribute anything interesting in

$$\overline{AP} + \overline{PA'} = \rho(\cos\theta + \cos\theta') - y(\sin\theta + \sin\theta') + \frac{y^4}{8\rho^3}(\tan\theta \sin\theta + \tan\theta' \sin\theta') + \cdots .$$

Now let us consider the resultant intensity at A' of light of wave length λ from all over the grating. If we let $\sigma\boldsymbol{\delta}_n (=\sigma\delta_n \exp 2\pi i(\text{path})/\lambda)$ represent the contribution of a single line of the grating to the total vector amplitude, then the quantity

$$I \equiv \left| \sum_n \sigma\boldsymbol{\delta}_n \right|^2 = \left| \sum_{n=-N/2}^{+N/2} \sigma\delta_n \exp\left\{\frac{2\pi i}{\lambda}\left[\rho(\cos\theta + \cos\theta') - n\sigma(\sin\theta + \sin\theta') + \frac{\eta^4\sigma^4}{8\rho^3}(\tan\theta \sin\theta + \tan\theta' \sin\theta')\right]\right\}\right|^2$$

may be called the intensity. Let us suppose that A' is the point on the Rowland circle where

$$\sin\theta + \sin\theta' = \frac{m(\lambda - \Delta\lambda)}{\sigma}, \tag{3}$$

i.e., where, following the ordinary grating condition, the mth order line due to light of wave length $(\lambda - \Delta\lambda)$ would have its central maximum intensity. Then

$$I = \left|\left[\exp\frac{2\pi i\rho(\cos\theta + \cos\theta')}{\lambda}\right]\sum_n \sigma\delta_n \exp\left\{\frac{2\pi i}{\lambda}\left[\frac{n\sigma m\Delta\lambda}{\sigma} + \frac{n^4\sigma^4}{8\rho^3}(\tan\theta \sin\theta + \tan\theta' \sin\theta')\right]\right\}\right|^2. \tag{4}$$

We can make the treatment quite general by the following changes of notation:

---

the present discussion. The essence of the design of the concave grating, as well as of the plane grating, is that the factors $\exp(2\pi i n\sigma m(\lambda - \Delta\lambda)/\lambda\sigma)$ in the expression for I below, are in phase for all integers n, if $\Delta\lambda = 0$; i.e., if A' is at the mth central maximum for wave length λ. The virtue of restricting A, A' to the Rowland circle is that under this restriction the second and third power terms cancel out. This shows why the fourth power term must be carried. The fifth power term is unimportant in the consideration of the resolving power (but see Section V for its effect upon the position of the central intensity maximum for a line). The introduction of the limit $H \to \infty$, below, is not justified physically, of course, so long as we have neglected higher powers. But in practical cases H is always less than 10, usually much less, and within this range our approximations seem reasonable.

$$\beta \equiv \left[\frac{4\lambda\rho^3}{\pi(\tan\theta\sin\theta+\tan\theta'\sin\theta')}\right]^{1/4} = \left[\frac{4\lambda\rho^4 rr'}{\pi(\rho^2-rr')(r+r')}\right]^{1/4} \tag{5}$$

$$\alpha \equiv \frac{2\pi m\beta\Delta\lambda}{\sigma\lambda}$$

$$\eta \equiv \frac{y}{\beta}, \quad H = \frac{Y}{\beta} \tag{6}$$

$$f(\eta) \equiv \beta\delta_n \tag{7}$$

where $\pm Y$ are the ordinates of the boundaries of that portion of the grating which we may wish to consider. The summation may be very closely approximated, when N is large, by the integral:

$$I = \left|\int_{-H}^{H} f(\eta)e^{i(\alpha\eta+\eta^4)}d\eta\right|^2. \tag{8}$$

We shall now assume for simplicity that all the δ_n's are equal (so that $f(\eta)$ may be factored out as a constant); the validity of this assumption will be discussed in Section VI (b).

The evaluation of this integral as a function of α (which for any line is proportional to $\Delta\lambda$) will give us an intensity curve for the light of wave length λ along the Rowland circle; this is what we need in order to determine the resolving power of the grating. We have found it best to evaluate this integral graphically by an extension of the Cornu spiral method by which the Fresnel integrals are often evaluated.[7] In the complex amplitude-vector plane, the two-parameter function

$$w(\alpha, H) \equiv u + iv = \int_0^H e^{i(\alpha\eta+\eta^4)}d\eta \tag{9}$$

is proportional to the amplitude of the light from the source A, scattered by that part of the grating betweeen the origin and H, to any point A' on the Rowland circle in the neighborhood of a central maximum (i.e., of $\alpha=0$) for that wave length. The distance of A' from the neighboring central maximum, and the grating width under consideration, determine the parameters α and H respectively.

Each of the family of curves of constant α shows the phase relations among the contributions to the amplitude from the various portions of the grating, for a fixed point A'. Four typical curves of this sort[8] are

[7] Cf. C. M. Sparrow, Ap. J. *49*, 65; 1919.

[8] The dashed circles tangent to the curves of constant α at the origin are the familiar curves $\int e^{i\alpha\eta}d\eta$ that one obtains by the usual analysis, neglecting the fourth power term. Now we can

given, with their α-values, in Fig. 2. At any distance H along the arc, the curve makes an angle $(\alpha H+H^4)$ with the u-axis. The radius of curvature, then, is $(\alpha+4H^3)^{-1}$, and one may approximate the curve as accurately as one pleases, graphically, by segments of circles. The ampli-

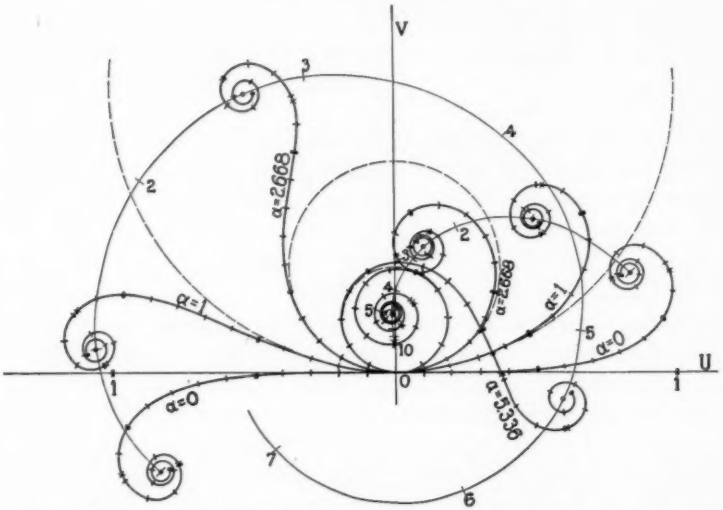

FIG. 2. *Amplitude spirals* $u=\int_0^H \cos(\alpha\eta+\eta^4)d\eta$, $v=\int_0^H \sin(\alpha\eta+\eta^4)d\eta$, *for typical values of* α. *For negative* α *the spirals are the same except for a reflection in the origin and an interchange of the branches. Values of* H *are plotted in tenths along each spiral. The values* $H=1.177$ *and* $H=1.50$, *marked with crosses, correspond to the grating widths that give the first maximum and first minimum amplitude, respectively, at the center of a spectral line,* $\alpha=0$. *The spirals curl up with increasing* α, *the one branch collapsing into the origin rapidly, the other slowly, both keeping their asymptotic points on the (light line) curves;* $H\to\pm\infty$. *The one branch lies entirely within, the other entirely without, the (dashed line) circle of radius* $1/\alpha$, *which would be the amplitude curve if the grating were plane. The failure of the spirals* $\alpha=\pi/1.177=2.668$ *and* $\alpha=2\pi/1.177=5.336$ *to close at* $H=1.177$, *where the circles would close, shows strikingly the effect the fourth power term has, even for such a moderate value of* H.

tude due to any region of the grating may be determined by measuring a chord of this curve. The general shape of the curves of constant H may

---

see the relationship between this work and the previous $\Delta(\text{path})<\lambda/4$ approximation (footnote 2). Treating the grating as though it were plane, but limited in width by the condition that the path discrepancy be less than $\lambda/4$, is identical (cf. equations (5) and (6) and Kayser, l.c., p. 458) with using segments of circles $\int_{-H}^{+H} e^{i\alpha\eta}d\eta$ in the amplitude plane, but limiting H to $(\pi/2)^{1/4}=1.120$. Paradoxically, the more accurate method (Fig. 2, supplemented by a series expansion for $w(0,H)$) shows that part of the *second* Huyghens zone up to $H=1.177=(0.611\pi)^{1/4}$, i.e., almost to $\Delta(\text{path})=5\lambda/16$, actually contributes *positively* to the amplitude at the central maximum.

be read from the curves of constant α in Fig. 2, each of which is furnished with an H scale. But in order to avoid confusion, only one curve (the limiting one, $H \to \infty$) of this family is drawn, as a light line. Analytically constructed according to the discussion in the next paragraph, it served in the construction of Fig. 2 as a convenient check on the accuracy of the curves of constant α.

$w(\alpha, \infty)$ may be evaluated[9] by contour integration, considering η for the moment complex, and using as the path of integration a sector, extending from the axis of reals through the angle $\pi/8$, of a circle of radius M about the origin. Since the integrand is analytic everywhere within a finite range, the integral about this contour is zero. The integral along the circle also vanishes as $M \to \infty$, so

$$w(\alpha, \infty) = \int_0^\infty e^{i(\alpha\eta+\eta^4)}d\eta = -e^{\pi i/8}\int_\infty^0 e^{(i\alpha\eta e^{\pi i/8}-\eta^4)}d\eta.$$

The integral on the right may be expanded as a Maclaurin's series in α, using the fact that

$$\frac{\partial^p w(\alpha, \infty)}{\partial\alpha^p} = e^{\pi i/8}(ie^{\pi i/8})^p\int_0^\infty \eta^p e^{(i\alpha\eta e^{\pi i/8}-\eta^4)}d\eta.$$

Hence

$$w(\alpha, \infty) = \sum_{p=0}^{\infty}\frac{\alpha^p}{p!}\frac{\partial^p w(0, \infty)}{\partial\alpha^p} = \sum_{p=0}^{\infty}\frac{(i\alpha)^p}{p!}e^{(p+1)\pi i/8}\int_0^\infty \eta^p e^{-\eta^4}d\eta$$

$$= \sum_{p=0}^{\infty}\frac{(i\alpha)^p}{4p!}e^{(p+1)\pi i/8}\Gamma\left(\frac{p+1}{4}\right).$$

This expansion was used in plotting $w(\alpha, \infty)$ in Fig. 2, over the range $0 \leqq \alpha < 7$.

From equations (8) and (9), it is clear that the intensity, due to any region of the grating symmetric about O, is:

$$I(\alpha, H) = \beta^2\delta^2\left|\, w(\alpha, H) - w(\alpha, -H)\,\right|^2. \tag{10}$$

The solid lines in Fig. 3 show the relative intensities:[10]

$$I_{rel}(\alpha, H) \equiv \frac{I(\alpha, H)}{I(0, H)} = \left|\frac{w(\alpha, H) - w(\alpha, -H)}{w(0, H) - w(0, -H)}\right|^2$$

[9] We are indebted to Prof. R. E. Langer for aid in putting this derivation into rigorous form.

[10] β is a function of $\Delta\lambda$ through its dependence upon $\cos\theta'$; hence it varies with α. The dependence is so slight, however, that we are quite well justified in calling β a constant for moderate values of α.

for a few values of H (i.e., for various grating widths), plotted against the abscissas αH. The dashed line is $I_{rel}(\alpha, \infty)$ plotted against α(instead of against αH).

With these intensity curves we can easily determine the resolving power of a concave grating as soon as we have a definition to tell us what it means for the lines to be resolved. Rayleigh's criterion, that two lines of equal intensity are theoretically resolved when the central maximum of one coincides with the first minimum (zero) of the other, can be ap-

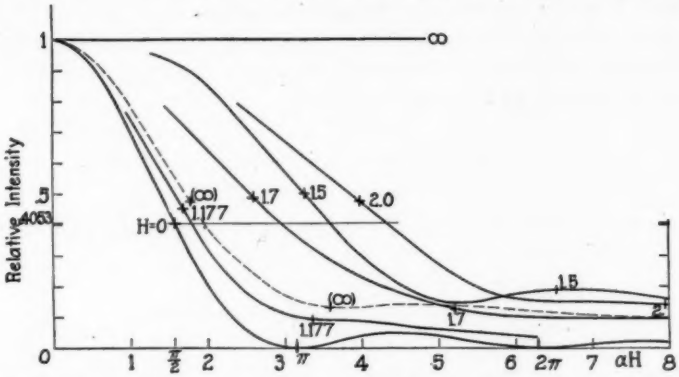

FIG. 3. *Relative intensity curves. The abscissa is proportional to distance along the photographic plate, on a different scale for each curve.*

plied to concave gratings only in the limiting case: $H \to 0$. Hereafter we shall say that two lines of equal intensity are resolved when the wavelength difference $\Delta_1 \lambda$ between them is such that the minimum total intensity between the lines is $8/\pi^2$ ($=0.8106$) as great as the total intensity of both at the central maximum of either of the lines.[11]

The value of α (or of αH) which would be necessary to separate two lines just resolved, in the above-defined sense, will be called α_1(or $\alpha_1 H$). The two crosses on each curve in Fig. 3 show the values of $\frac{1}{2}\alpha_1 H$, and $\alpha_1 H$, found by trial. The resolving power $R \equiv \lambda/\Delta_1\lambda = 2\pi m\beta/\sigma\alpha_1 = mN\pi/\alpha_1 H$.

[11] It is often possible to resolve two lines with $\Delta\lambda$ considerably smaller than $\Delta_1\lambda$. The fraction is calculable in special cases from the "undulation condition," C. M. Sparrow, Ap. J. *44*, 76; 1916. We use a new criterion for resolution rather than Sparrow's because it seems at least as useful practically, and we prefer to extend rather than abandon Rayleigh's classical one. Several workers, e.g., A. Schuster, Ap. J. *21*, 197; 1905 and S. K. Allison, Phys. Rev. *38*, 203; 1931, have used simpler criteria, which are safe only when the outer portion of the intensity pattern can be neglected, which is far from true for the concave grating (see Fig. 3). It is well known that when two lines are nearly superimposed their maxima may be shifted, and the problem is further complicated by photographic and psychological phenomena; but here we are neglecting all these complications.

Since mN is the resolving power of the plane grating of the same width and the same number of lines, $\pi/\alpha_1 H$ is something like an efficiency for the concave grating. Hence π/α_1 may be called H_{eff}, the effective value of H.

Fig. 4 shows H_{eff} plotted as a function of H. The curve shows that the resolving power is approximately that of a plane grating[12] for values of H up to the neighborhood of unity, and increases up to an optimum value of H, $H_{opt}=1.18$, at which point $H_{opt_{eff}}=1.09$. Larger values of H, however, cause no larger values of H_{eff}, which oscillates about 0.88 as the width of the grating increases. Thus, to find the actual resolving power of a certain grating at a certain angle of incidence, for a given order and wave length, it is only necessary to calculate the value of H from equations (5) and (6), to find H_{eff} from Fig. 4, and to multiply the plane grating resolving power, mN, by the ratio H_{eff}/H. In case H is

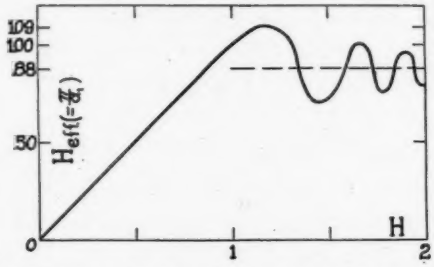

FIG. 4. *H_{eff} plotted against H. The ratio of ordinate to abscissa gives the ratio of the resolving power of the grating to mN.*

much greater than unity, one may approximate the value of the resolving power by taking H_{eff} to be 0.88, its asymptotic value. It is readily seen from equation (5) that when r and r' are of the order of magnitude of ρ, as is the case in most of the older concave grating mountings, β is so large that $H<1$, and $H_{eff} \cong H$. Then the resolving power is very nearly equal to that of the plane grating of the same width, which is the usual approximation.

The usual results of the theory of the perfect plane grating illuminated by parallel light may be obtained by considering the limiting case of a concave grating, where ρ increases indefinitely. For instance,

[12] In the $\Delta(\text{path})<\lambda/4$ approximation, $H_{eff}=H$ up to $H=(\pi/2)^{1/4}=1.120$, the end of the first Huyghens zone, beyond which point H_{eff} is constant. For such a simple approximation this gives very good results. The ratio, R (simple approximation): R (this paper) is always somewhat more than unity. For all $H<1.2$ it is never more than 1.05, and for $H\to\infty$ it is 1.27. The worst discrepancy is in the neighborhood of $H=1.5$, where the ratio is 1.6.

we have immediately from equations (5) and (6), that for a plane grating $H=0$, and from the calculations for I_{rel}, upon which Fig. 3 is based, that the diffraction pattern from a plane grating is the one made so familiar by the fundamental work of Lord Rayleigh: $(\sin \alpha H/\alpha H)^2$.

II. Optimum Width

The optimum width of the grating:

$$2Y_{opt} = 2\beta H_{opt} = 2.36\beta.$$

can be calculated from equation (5). In most cases where it is of interest it can be roughly interpolated from Table 1, which gives $2Y_{opt}$ in centimeters for several typical values of θ (or θ', since the two angles enter symmetrically into the expression for β), m/σ, and λ, for a one meter grating ($\rho=100$ cm). One can easily find the optimum width for another radius by multiplying the value found from Table 1 by $(\rho/100\text{ cm})^{3/4}$. It will be noticed that except where θ is small, $2Y_{opt}$ is practically independent of m and σ. The optimum resolving power is

$$R_{opt}=(1.09/1.18)\cdot 2Y_{opt}\cdot m/\sigma=0.92\cdot 2Y_{opt}\cdot m/\sigma.$$

For a grating much wider than $2Y_{opt}$.,

$$R=(0.88/1.18)\cdot 2Y_{opt}\cdot m/\sigma=0.75\cdot 2Y_{opt}\cdot m/\sigma.$$

Table 1 shows that for large angles of incidence it is a positive disadvantage, insofar as resolving power is concerned, to have greater angles

TABLE 1. *Values of $2Y_{opt}$ (cm) for a one meter grating.*

$m/\sigma=6000$ cm^{-1}						$m/\sigma=24000$ cm^{-1}					
	$\lambda=0$	10	100	1000	5000A		$\lambda=0$	10	100	1000	5000A
$\theta=0°$	0/0	57.3	32.2	18.1	12.8	$\theta=0°$	0/0	28.7	16.1	9.0	—
45°	0	1.29	2.30	4.19	6.85	45°	0	1.29	2.31	4.48	6.67
80°	0	0.77	1.40	2.65	4.23	80°	0	0.77	1.45	2.80	4.32
88°	0	0.53	1.03	1.88	2.86	88°	0	0.55	1.05	1.91	2.87
90°	0	0	0	0	0	90°	0	0	0	0	0

of incidence and excidence than are necessary for sufficient reflection to obtain a satisfactory photograph. As an extreme example of the danger of disregarding this fact, we may call attention to attempts that have been made to photograph "inside orders," i.e., lines between the central image and the grating at grazing incidence. It may readily be shown, by differentiating equation (11) below, that the general formula for the dispersion D of a concave grating is $D=dq/d\lambda=\rho m/\sigma\cos\theta'$, where $dq(=$

$-\rho d\theta'$) is a distance element measured along the Rowland circle, i.e., along the photographic plate. Thus the dispersion increases rapidly for inside order lines as $\cos\theta' \to 0$. But always the inside order lines have been hazy and the results inferior to those obtained with outside orders. Now one can see a sufficient reason for these failures: $\lim_{\theta' \to \pi/2} R = 0$, although $\lim_{\theta' \to \pi/2} D = \infty$!

The optimum width has been called the optimum, purely on the basis of its resolving power. Equation (10) gives the absolute value of

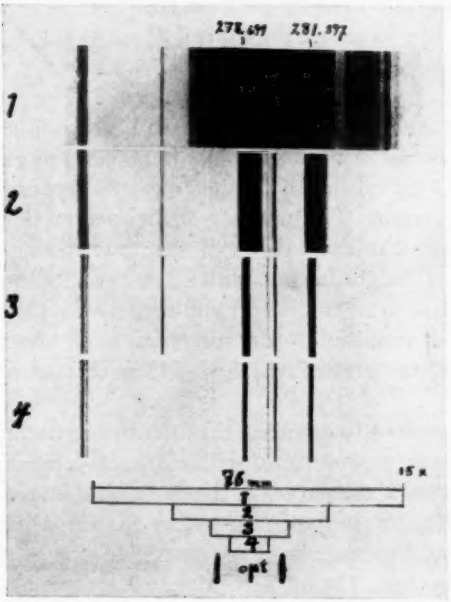

FIG. 5. *Intense spectral lines from wide and narrow gratings. Exposures (1) to (4) were identical except that the width of the exposed portion of the grating was varied as shown schematically in the lower part of the figure. The distance marked "opt" represents the calculated optimum width.*

the intensity at any point (in the neighborhood of a line) on the Rowland circle which is equal to the constant $\beta^2\delta^2$ times the square of the appropriate distance in Fig. 2. Thus we may determine the central maximum intensity of a line as a function of H, from the $\alpha = 0$ spiral. The graph of this relationship begins as a parabola, but for values of H greater than about 1, it follows remarkably closely the contour of the (H_{eff}, H) curve, Fig. 4, and the optimum already discussed is practically the optimum for intensity as well as for resolving power.

III. ELIMINATION OF GRAZING INCIDENCE GHOSTS

Some experiments in Uppsala with a Wood glass grating ($\rho = 100$ cm, $\sigma^{-1} = 11.83 \cdot 10^3$ cm^{-1}, $2Y = 7.6$ cm, $\theta = 84.4°$) have shown that the employment of gratings of much greater width than $2Y_{opt}$ is responsible for the scattered light which, for large angles of incidence, appears conspicuously in fluted patterns like ghosts around strong lines. Fig. 5 shows the appearance of the *Al V* doublet at 280A photographed by means of a grating whose width was adjusted by screening, as follows:

(1) $2Y = 7.6$ cm, $H = 5.4$
(2) $2Y = 4.0$ cm, $H = 2.8$
(3) $2Y = 2.0$ cm, $H = 1.4$
(4) $2Y = 1.0$ cm, $H = 0.7$

The calculated $2Y_{opt}$ for that wave length is about 1.68 cm, and from the figure it may be seen how the last indications of ghosts disappear between 2 and 1 cm width. All the spectrograms were obtained with the same time of exposure. The intensity of the spectral lines is not appreciably affected by screening. We have seen that theoretically the light from the parts of the grating outside $2Y_{opt}$ contributes neither to the resolving power nor to the intensity, and here we see that empirically it appreciably adds confusion to the spectrum; so we conclude that for a clean spectrum, the grating width should never considerably exceed $2Y_{opt}$.

It is not convenient to calculate the intensity pattern to be expected theoretically from a wide grating, for direct comparison; however qualitative studies of the nature of the theoretical intensity patterns in a region considerably beyond that shown in Fig. 3 have been made (graphically, and by expanding the right hand side of equation (9) in negative powers of α). The intensity due to a grating much wider than $2Y_{opt}$ decreases very much more slowly with increasing distance from the center of the line, than that due to a plane grating under similar conditions. The slowness of this decrease would be in agreement with a general blackening over a wide region in the neighborhood of a very intense line. But (neglecting higher powers of H than the fourth) there is no place in the theory of the perfect concave grating for the marked flutings.[13] So these may properly be called ghosts, although they fail completely to show the simple regularity ($\Delta\lambda/\lambda$ independent of λ) in wave-length intervals that is characteristic of the usual Rowland ghosts from plane and narrow concave gratings.

[13] The flutings are much too far apart to be accounted for as secondary maxima of the sort shown in Fig. 3.

IV. ECONOMIES IN RULED AREA

In Sections II and III we have seen the advantages of limiting the widths of gratings in some cases. Now we shall see that, although extra length is not, like extra width, positively harmful, there are cases where the rulings may be made much shorter than is now customary, without detriment and with considerable saving in wear on the ruling diamond.

In order to determine the useful length of rulings for a grating, let us consider the three dimensional problem (c, c', $z \neq 0$). Then, if in expanding $\overline{AP}$ and $\overline{PA'}$ to find the path, we keep terms up to the second power of c and z, we find that the path $\overline{AP}+\overline{PA'}$ is given by:

$$\overline{AP} + \overline{PA'} = r + r' - y(\sin\theta + \sin\theta') + \left(\frac{c^2}{2r} + \frac{c'^2}{2r'}\right) - z\left(\frac{c}{r} + \frac{c'}{r'}\right) + z^2\left(\frac{\sin^2\theta}{2r} + \frac{\sin^2\theta'}{2r'}\right) + \cdots .$$

Now, however, one must not only sum over all the rulings of the grating (as before), but also integrate over the length of each ruling in order to obtain the total contribution of the grating to the amplitude at A'. This amounts to multiplying the result obtained before by a factor:

$$\exp\left\{-\frac{2\pi}{\lambda}\left(\frac{c^2}{2r} + \frac{c'^2}{2r'}\right)\right\} \int_{-z}^{+z} \exp\left\{\frac{2\pi i}{\lambda}\left[-z\left(\frac{c}{r} + \frac{c'}{r'}\right) + z^2\left(\frac{\sin^2\theta}{2r} + \frac{\sin^2\theta'}{2r'}\right)\right]\right\} dz.$$

This integral is of a type similar to the one we have been studying, and can be represented in the complex plane as a spiral in a similar manner. Hence, just as in the case of $\int e^{i(\alpha\eta+\pi\eta^2)}d\eta$, we see that the modulus of this integral reaches a maximum when the coefficient of z is zero; i.e., when $c/c' = -r/r'$. That is merely the statement that the intensity at c' is greatest when c, 0, and c' all lie in a plane normal to that tangent to the grating at its center. Except when $\theta,\theta' \to 0$, the maximum is not very marked, i.e., the grating as a mirror is very astigmatic; for, as we shall soon show, the Huyghens zones on the grating are very narrow in the z-direction, so that only a small portion of the grating is effective in reflecting light to c'. Hence a shift of the grating in the direction of its rulings should make little difference in the intensity at c' (since the outer Huyghens zones count but little), although the maximum is shifted.

The width of any one of the Huyghens zones on the grating, whose reflected light varies by not more than π in phase at the image, can be found from the formula[14] for the coordinates of the zone edges:

$$z_j = \pm \left[\frac{(j - \frac{1}{2})\lambda\rho}{\tan\theta \sin\theta + \tan\theta' \sin\theta'} \right]^{1/2}.$$

Except in the case of nearly normal incidence and excidence, $|z_1| \sim 10^{-1}$ cm or less. For grazing incidence, we may have $|z_1| \sim 10^{-3}$ cm. This narrowness of the zones enables us to use simple geometric optics (save when θ and θ' are both small) in finding the smallest desirable length $2Z$ of the rulings, if we make a slight extra allowance so as not to cut off the grating within the first few zones associated with any of the rays.

Thus, when the slit is illuminated by a wide-angle lens, the lengths $2C$ and $2C'$, respectively, of the slit and the lines desired on the photographic plate, determine the half-length of the rulings as follows: $Z = (C'r + Cr')/(r + r')$.

When the slit is illuminated only by direct rays from the source, as is necessary in the extreme ultraviolet, it is better, for these considerations of length, to treat the actual source, rather than the slit, as the source. Let us say that the source is distant r_0 (along r extended) from O, and that its length is $2C_0$. Then r and C must be replaced by r_0 and C_0 in the above formula for Z. If C_0 is very small, and if one wishes to photograph down to very short wave lengths, then the expression for the smallest desirable half-length of the rulings reduces to $Z = C'/2$, and the smallest desirable half-length of the slit is $C = C'(r_0 - r)/2r_0$. In ordinary cases $2C$ and $2Z$ need not be more than a few millimeters.

V. INEXACTNESS OF THE GRATING CONDITION EQUATION

The equation

$$\sin\theta + \sin\theta' = m\lambda/\sigma \tag{11}$$

determines a point in the Rowland circle which is ordinarily taken as the position of a line of wave length λ. Strictly speaking, however, the position of a line[15] is, in the language of this investigation, determined by the value of α, which we shall call α_0, which gives the principal maximum of the intensity

[14] Kayser, l.c., p. 459.

[15] i.e., the value of $\Delta\lambda$ in equation (3) corresponding to the shift in the intensity maximum from the position given by equation (11).

$$I_{exact} = \left| \int_{-H}^{+H} f(\eta) e^{i(\alpha\eta + \beta\eta^4 + \gamma\eta^5 + \cdots)} d\eta \right|^2 \tag{12}$$

where γ and the coefficients of higher powers of η can be found from equations (2) and (5). Making the usual approximation, $f(\eta) =$ a constant, and neglecting terms of higher than the fourth power in η, in Section *I* we found $\alpha_0 = 0$, i.e., found equation (11) to be exact. If we now include the fifth power term, still neglecting higher powers of η, the expression (12) may be evaluated as a multiple series. Now $\gamma(\sim\beta \tan\theta/\rho$ or $\beta \tan\theta'/\rho)$ is generally small, rarely as much as 0.1. Also, from the nature of the spirals represented by the integral in equation (12), it can be seen that α_0 will be of the same order of magnitude, at least for moderate values of H. Therefore we may neglect terms of higher power than the first in α and γ in the expansion of equation (12). Differentiating with respect to α and setting the result equal to zero, we find that $\alpha_0 = -\phi(H) \cdot \gamma$, where $\phi(H)$ is a double series in H, not readily evaluable. When $H \to 0$, $\phi \leqq 3/7\ H^4$; when $H \to \infty$, $\phi \leqq H^4$; and a detailed calculation for the case when $H = H_{opt}$ gives $\phi = 0.3H^4$. So we feel justified in stating that ϕ is of the order of H^4. Therefore, since

$$\gamma = \frac{\beta(\tan^2\theta \sin\theta + \tan^2\theta' \sin\theta')}{\rho(\tan\theta \sin\theta + \tan\theta' \sin\theta')}, \text{ and } \alpha = \frac{2\pi m\beta}{\sigma\lambda} \cdot \Delta\lambda$$

it seems safe to say that the error in the determination of the wave length of a line by equation (11) is

$$\Delta_0\lambda \sim -\frac{H^4\sigma\lambda(\tan^2\theta \sin\theta + \tan^2\theta' \sin\theta')}{2\pi m\rho(\tan\theta \sin\theta + \tan\theta' \sin\theta')}.$$

An idea of the magnitude of $\Delta_0\lambda$ can be gained from the errors calculated for the first order spectrum of the grating whose resolving power was recorded in Fig. 6. Making use of the exact value of ϕ obtained above for H_{opt}, we obtain:

θ	λ	$\Delta_0\lambda$
0°	5000A	0.0003A
45	5000	0.0007
84.6	100	0.00015
84.6	1000	0.0015
84.6	5000	0.008

The error increases with grating width, wave length, and angle of incidence. The values given in the table are not the errors to be expected in

actual cases, for at 0°, H is ordinarily much less than H_{opt}, and $\Delta_0\lambda$ correspondingly smaller; while at large angles of incidence, H is liable to be larger than H_{opt}, and $\Delta_0\lambda$ perhaps several times as large. Moreover, lines are commonly measured by comparison with standards, and the error is such a slowly changing function of the wave length that the discrepancy is trivial in all cases where neighboring lines of the same order are compared. In the comparison of lines of different orders it is not necessarily trivial, but even here it enters only through the dependence of ϕ upon H^4. (For lines of different orders at the same place on the photographic plate, H^4 is proportional to the order m). In the latter case, though the discrepancy is usually too small in order of magnitude to be appreciable, it might have to be borne in mind in some cases in the determination of wave-length substandards.

VI. THE SPECTROGRAPH

Up to this point we have been considering properties of the grating. Now we shall discuss the concave grating spectrograph as a whole. The results obtained above are valid for the spectrograph only if the experimental conditions are ideal with respect to: (a) adjustment of the point of tangency of the Rowland circle at the center of the grating surface, (b) equality of illumination at A' from all parts of the grating, and (c) narrowness of the slit. The first condition is rarely fulfilled in practice, and the other two, never.

(a) By the usual methods of adjustment the photographic plate is brought quite accurately into focus with the slit; i.e., both are on a circle of radius $\rho/2$ tangent to the grating circle. The common tangent, however, is not necessarily the one parallel to the axis (the y-axis in Fig. 1) along which the constant grating interval σ is measured. Let us consider now the effect of a small displacement of the point of tangency as though the Rowland circle in Fig. 1 were rolled along the grating circle; so that the new common tangent, say at (x_0, y_0), would be at an angle $\epsilon = -\arcsin(y_0/\rho) \cong -y_0/\rho$ with the y-axis. Equations (2) et seq. give the path approximately in terms of a new ordinate measured from (x_0, y_0) as origin. Calculating the path anew in terms of the ordinate measured from the center of the grating, we find terms of every power in y. The new terms of powers less than the fourth have two effects upon the intensity patterns. They introduce a shift in the positions of the lines, which, like the $\Delta_0\lambda$ of Section V, is unimportant in ordinary relative measurements; and they alter the shapes of the spirals to such an extent that if $|y_0|$ is as much as $Y_{opt}/4$, about as much aberration is introduced

in the region $|\eta| < H_{opt}$ as Fig. 2 shows. (The aberration in Fig. 2 is due to the fourth power term, for the case $y_0 = 0$). So, in order to take advantage of the property of the Rowland circle whereby aberrations of lower order than the fourth cancel, we must have $y_0 << Y_{opt}/4$. In other words, it is not sufficient, for the best resolving power, to have the plate in focus, but the common tangent to the two circles must be brought close to the center of the grating compared with the distance Y_{opt}.

(b) In equation (8) it was expedient to assume that the contributions δ_n of all the lines of the grating to the amplitude at A' were equal ($f(\eta)$ constant, equation (7)). The actual dependence of δ_n upon n is in general quite complicated. The effect of its variation upon the shape of Fig. 2, is to compress some portions of each spiral with respect to other portions. Faintness of the light from one end of the grating, for instance, increases the curvature of the corresponding end of each spiral. If the illumination is symmetric, i.e., if $\delta_{-n} = \delta_n$, the position of the central maximum is the same as that given in the ordinary analysis (except for terms of still higher order than the fourth—see Section V), but the intensity pattern, and hence the resolving power, may be affected. Non-symmetric illumination, in general, shifts the maximum. But when the illumination from the first few Huyghens zones (corresponding to the first few turns of the spirals) is fairly even, the variation is probably so slight as not to affect seriously the essential results of the analysis. But it is probably enough to alter the shape of the resolving power curve (Fig. 4) after the first few oscillations, usually smoothing it out and shifting the maxima somewhat, so there is no practical use in calculating the fine structure of Fig. 4 when H is greater than, say, 2. It is for this reason that the asymptotic value, $H_{eff} = 0.88$, was used in Fig. 6.

(c) The finite slit width of a real concave grating spectrograph has two closely related effects upon the resolving power[16] of the instrument. First, purely geometric considerations of the angles subtended at the grating by the slit and by its image, show that the two rays from the opposite edges of the slit are separated by a distance $s/\cos\theta'$ on the photographic plate, corresponding to a wave-length range $\Delta_1\lambda_{geom} = s/D \cos\theta'$

[16] We might be expected to express the resolving power or "purity" of the instrument in terms of Schuster's "purity factor" (Encyclopedia Brittanica, 9th ed., "Spectroscopy," and Ap. J. *21*, 197; 1905). But the complicated case of the concave grating spectrograph does not seem to be amenable to such simple treatment, so we have been compelled to limit our considerations to cases where either the slit or the grating is predominant in limiting the instrument's resolving power. We are indebted to Drs. R. O. Rollefson and A. E. Whitford for profitable discussions of the case of finite slit width.

$=s\sigma/\rho m$, where s is the slit width. Second, the real grating spectrograph presents a complicated problem of two diffractions in series: at the slit, and at the surface of the grating. We are justified in adding the amplitudes vectorially, as in Fig. 2, only insofar as the light emerging from the slit is coherent. The theory is exactly valid only when $s\rightarrow 0$, the slit giving rise to a coherent circular wave front exactly as though it were a source. When $s\neq 0$, monochromatic light falling upon the slit from a certain direction diverges from it in a coherent beam of angular width approximately $2\lambda/s$ (between the principal intensity minima), covering a range $2Y_{coh}=2\rho\lambda/s$ upon the grating. Then any point at the slit, considered as a source, gives rise to a line on the photographic plate whose breadth corresponds[17] to the wave-length range

$$\Delta_1\lambda_{coh}=\frac{\lambda\sigma}{2Y_{coh}m}=\frac{s\sigma}{2\rho m}=\tfrac{1}{2}\Delta_1\lambda_{geom}.$$

The two effects combine to form a line consisting of the Rayleigh diffraction pattern of width $\frac{1}{2}\Delta_1\lambda_{geom}$, integrated over the range $\Delta_1\lambda_{geom}$. The method used in determining the $\alpha_1 H$'s in Fig. 3, shows that this line has a breadth $\Delta_1\lambda_{slit}=1.10\Delta_1\lambda_{geom}=1.10\ s\sigma/\rho m$. In any case, then, the resolving power of a concave grating spectrograph can not be greater than $R_{slit}\equiv\lambda/\Delta_1\lambda_{slit}=0.91\rho\lambda m/s\sigma$. So, if the grating resolving power theory is to apply to our spectrograph, the slit width should be so small that R_{slit} is at least somewhat [18] greater than the R found above for an infinitesimal slit. But if R_{slit} is as much as, say, twice R ($s\sim\rho\lambda/4Y_{opt}$), further reduction of the slit width offers no advantages to offset the dis-

[17] In this analysis we have treated the line on the photographic plate as though it were due to diffraction from a uniformly lighted plane grating of width $2Y_{coh}$, neglecting: (1) the variation of δ_n within the region $2Y_{coh}$ due to the shape of the slit diffraction pattern on the grating; and (2) the higher order aberrations in the grating which would give rise to a $2Y_{coh_{eff}}<2Y_{coh}$. These approximations are justified by the result below, that the whole diffraction pattern from the slit broadens the geometric image from the slit by only ten percent.

[18] It might be worth while to consider the possibility of improving the resolving power of the system for a narrow wave-length region by deliberately widening the slit. The relationships that allow this possibility can be seen best by reference to the example, Fig. 6. The ordinates, for each wave length, are proportional to H. In the right hand part of the picture, the ratio between the width of the grating ("plane grating") and the effective width curve drawn ("concave grating, asymptote") equals $H/0.88$. But in the left hand part, the effective width, as limited by the size of the slit, takes the place of the whole width in determining H. So, near the intersection of the "concave grating" curve and the "slit" curve, H is small again, and relatively large oscillations of H_{eff} about the asymptotic value occur. The resolving power in the neighborhood of the intersection of the theoretical curves for the slit and for the grating, can not very well be discussed in detail, on account of the complicated nature of the illumination function δ_n. But it might be improved by experimental comparison for different values of s.

advantages of inconvenience, clogging, and reduced intensity always encountered with very narrow slits. For the very shortest wave lengths, the slit width required by this condition is smaller than can be used in practice (see Fig. 6), so the width of the slit must be the determining factor in the resolving power.[19]

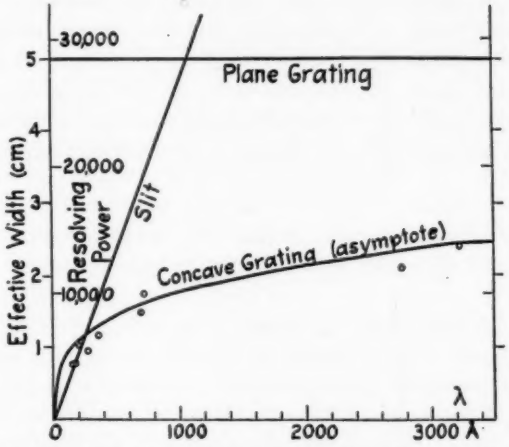

FIG. 6. *Experimental test of the resolving power. Experimentally resolved line pairs are plotted as circles. The theoretical value is given, for any wave length, by the lowest of the curves.*

The observed values of the resolving power in the first order of a grating used at grazing incidence at Uppsala ($\rho = 101.25$ cm, $\sigma^{-1} = 5710$ cm^{-1}, $2Y = 5$ cm, $s = (2.0 \pm 0.2) \cdot 10^{-4}$ cm, $\theta = 84.6°$) are compared, in Fig. 6, with the theoretical resolving power curves:

$$R_{plane\ grating} = mN,$$

$$R_{concave\ grating} (\equiv R, \text{ above}) = mNH_{eff}/H,$$

and

$$R_{slit} = 0.91\rho\lambda m/s\sigma.$$

The theoretical resolving power for any wave length is given by the lower of the two values, "concave grating" and "slit." Because of uncertainties in the illumination function δ_n, discussed in paragraph (*b*),

[19] At the shortest wave lengths, the increased penetrating power of the rays would be expected to cause an asymmetric broadening of the lines, proportional to sin θ' and to the penetration of the rays, and limited (unless there were considerable reflection at the surface of the glass) by tan θ' times the thickness of the photographic (Schumann) emulsion. Also, the photographic resolving power of the plate itself might limit the resolving power of the system. In our example neither of these influences is important.

the concave grating curve uses 0.88, the asymptotic value of H_{eff}, rather than the actual oscillating values for finite H, so the experimental values might be expected to be somewhat scattered above and below the curve. We must not forget, however, that the experimental values were determined from the separations of actual spectral lines; we should expect, in general, that line pairs closer together than those observed might be resolved, if they existed. This makes the recorded experimental resolving power in each case smaller than the real one. The agreement between experiment and theory may be said to be, on the whole, quite satisfactory. The slight excess of the experimental over the theoretical values, for the lowest wave lengths, may be attributed to the uncertainty in the slit width.

Ultraviolet Rays and Works of Art. By JAMES J. RORIMER, 1931, 61 pp., 47 figures, $2.50 in cloth, $2.00 in paper, Metropolitan Museum of Art.

As the author says, this book is merely an introduction to ultraviolet radiation as an aid in determining the age and condition of works of art and not an exhaustive study of the subject. The same work could have been done a score of years ago and it seems strange, considering the value of works of art, that ultraviolet radiation as an aid in establishing identity, fraud and repairs has been studied so little. The chief value in this little book lies in the forty-two half-tone plates of art objects, in each of which the photographic appearances under ordinary artificial light and ultraviolet radiation are compared. The photographs include objects in stone, ivory, bone, ceramics, textiles, prints, glass, enamel, wood and painting. The textual comments are valuable supplements to the illustrations.

The first chapter, dealing with ultraviolet radiation and apparatus, could easily have been more comprehensive and additional data pertaining to filters and sources could have been included. One is somewhat shocked at Diagram 1 which shows a prism dispersing "light" into the entire gamut of wave lengths (or frequencies) from cosmic rays to electrical waves. In general, the author presents the technical aspects commendably and doubtless satisfactorily for those to whom he introduces the subject.

M. LUCKIESH

DETERMINATION OF THE SPECTRAL COMPOSITION OF X-RAY RADIATION FROM FILTRATION DATA*

By Ludwik Silberstein

[Kodak Research Laboratories, Rochester, N. Y.

Received February 5, 1932]

The radiation emitted by an x-ray tube is complex or heterogeneous, consisting of a continuous spectrum which, under usual technical conditions, covers a range from one or a few tenths up to 1.2 or 1.3 angstroms. The 'quality' of the radiation, especially with regard to its therapeutical applications, depends upon the extent of the spectrum and the distribution of energy over its whole range, in brief, upon the spectral composition of the radiation. The direct determination of the composition of a sample of x-rays offers considerable experimental difficulties. On the other hand, the so-called filtration or absorption curve of such a sample of radiation can be obtained with comparative ease. Thus the problem of determining, mathematically, the former from the latter naturally suggests itself. The purpose of the present paper is to give an approximate, practicable method of solving it and to illustrate the method on a number of concrete examples.

The problem can be stated as follows: A sample of x-ray radiation has been filtered through foils of a substance, as e.g., aluminium or copper, whose absorption coefficient is an empirically determined function of the wave length. The total intensity of the transmitted radiation has been measured for a set of different thicknesses of the filter and thus the 'filtration curve' of the radiation (intensity plotted against thickness) has been constructed. It is required to determine the spectral composition of that sample of radiation.

In symbols, let x be the thickness of the filter, $\mu = \mu(\lambda)$ its absorption coefficient for homogeneous radiation of wave length λ, and $f(\lambda)d\lambda$ the (unknown) partial intensity or energy contained within the infinitesimal portion λ to $\lambda + d\lambda$ of the spectrum of the original radiation sample, so that its total intensity is $I(o) = \int f(\lambda)d\lambda$. Then, since the validity of the simple exponential law for each partial homogeneous radiation, expressed by the attenuation factor $e^{-\mu x}$, can be taken as experimentally well established, the total intensity $I(x)$ of the transmitted radiation is

* Communication No. 491.

$$\int_0^\infty e^{-\mu(\lambda)x} f(\lambda) d\lambda = I(x), \tag{1}$$

where, assuming the absence of any information as to the actual spectral extension of the sample, the extreme values 0 and ∞ have been taken for the limits of the integral. (This interval will be narrowed down presently.) The problem, then, is: Given $I(x)$ and $\mu(\lambda)$ as functions of their arguments, find $f(\lambda)$.

Eq. (1) is an integral equation of what is called the first kind, with $I(x)$ as the given, $f(\lambda)$ as the unknown function, and $e^{-\mu(\lambda)x}$ as the 'kernel' which can again be considered as a given function of x, λ.

It certainly is a given analytical function as regards x, though not so with regard to λ. The absorption coefficient is usually represented by the empirical cube-formula which can be written

$$\mu = \alpha + \beta\lambda^3$$

where, for a given element, α is constant throughout and β remains so up to the first critical limit K and then jumps to another constant value[1] which it retains up to the next L-limit, and so on, and it is claimed[2] that this formula expresses "fairly satisfactorily" the absorption by all elements of atomic number greater than 5 for $\lambda = 0.1$ up to 1.4A. As a matter of fact, however, this formula gives only a very rough representation, leaving in the case of aluminium, for instance, huge deviations from the observed values.[3] The case of copper is not much better. Accordingly, no use will be made here of the cube-formula, and the required μ-values will be taken from the available table of experimental determinations of this coefficient.

There is, however, at any rate a one-to-one correspondence between the μ- and the λ-values, expressible tabularly or graphically, say. Hence one may without any further clauses introduce μ instead of λ as the integration variable. Let $f(\lambda)d\lambda/d\mu = \phi(\mu)$. Then, and since to all purposes $\mu(\infty) = \infty$, $\mu(o) = 0$, equation (1) will become

[1] For aluminium $\lambda_k = 7.59$ A, and for copper $\lambda_k = 1.38$A, so that for these most important filters the jumping-clause would be superfluous within 0.1–1.35A, which is the whole interval of practical interest in our connection.

[2] E.g. by A. H. Compton, "X-rays and Electrons," 1926, p. 189.

[3] According to the cube-formula the ratio of differences $\Delta\mu : \Delta(\lambda^3)$ ought to be constant. Now, e.g., for $\lambda = 0.1$ 0.15 0.20 0.25 0.30 0.40 0.50 0.60 0.70 0.80 0.90 1.0 1.1 1.32 the observed values are $\mu/\rho = .164$ .201 .269 .370 .531 1.05 1.91 3.18 5.00 7.50 10.3 13.8 20.0 31.5 whence one finds for the said ratio of differences between contiguous items (divided by a constant, 10ρ) the values 1.56 1.47 1.32 1.41 1.40 1.41 1.40 1.43 1.48 1.29 1.29 1.49 1.19 which show huge oscillations.

$$\int_0^\infty e^{-x\mu}\phi(\mu)d\mu = I(x), \qquad (L)$$

an integral equation for the distribution function $\phi(\mu)$, with a much simpler kernel, symmetrical in the two variables. But the solution of the equation, even in this reduced form, by any of the methods developed in the theory of integral equations would be exceedingly laborious and, in practice, scarcely feasible at all. Such are in general the solution methods of that theory, based on series developments and implying the evaluation of a succession of integrals of increasing multiplicity.[4] Nor does there seem to be a royal road to a rigorous solution in our present case, (L). In fact, although the very same transformation, $T\phi = \int_0^\infty e^{-xu}\phi(u)du$, has already been introduced by Laplace as an auxiliary for solving differential equations and has been studied extensively by Abel, Murphy, Lord Kelvin, Borel, and others, the inverse transformation T^{-1} (which would at once solve our problem) is not, to my knowledge, available in convenient form.[5]

If, however, an approximate solution only is aimed at, that is to say, the determination of a moderate number of discrete ordinates of the spectral curve, then the following algebraical procedure readily suggests itself. (Fredholm's pioneer work in the field of integral equations is essentially based upon just such a procedure pushed to the limit.)

Returning to (1), let $\lambda = a$ to b be the whole interval in which the presence of perceptible radiation intensities may at all be expected, so that the equation will become

$$\int_a^b e^{-\mu(\lambda)x}f(\lambda)d\lambda = I(x). \qquad (1')$$

It is a well established fact that the continuous x-ray spectrum ends

[4] Actually these methods have been constructed mainly for the integral equations of "the second kind," viz. of the type

$$f(x) - \sigma\int_a^b k(x, y)f(y)dy = F(x),$$

where σ is a parameter and $f(x)$ the unknown function, whereas not much attention has been paid by the mathematicians (except Volterra) to the equations of the first kind. In the case of the former, power series of the parameter σ are used.

[5] *Note added Jan. 30, 1932.* Since this has been written the writer has obtained, with the kind aid of Dr. H. Batemau, a rigorous solution of the integral equation (L) for a certain class of functions $I(x)$ which cover quite closely most of the observed filtration curves. This has enabled him to derive with ease the complete spectral curves for radiation samples whose filtration curves are of such a type. This method and its practical applications will be set forth in a paper which is now being prepared.

sharply at the limiting wave length λ_m determined by the quantum relation

$$h\nu_m = \frac{hc}{\lambda_m} = \tfrac{1}{2}mv^2 = Ve,$$

where e is the absolute value of the electronic charge, V the potential applied to the emitting tube, h and c Planck's constant and the light velocity, or, if λ is expressed in angstroms and V in kilovolts,

$$\lambda_m = \frac{12.34}{V}. \tag{2}$$

This then can be taken for the lower limit a. As to the upper limit, all cases occurring in technical applications will be amply covered by taking $b = 1.3$A at the utmost. Now, divide the total interval into a number n of equal parts, $\Delta\lambda$, and let $\lambda_1, \lambda_2, \cdots \lambda_n$ be the mid-points of these partial intervals. Then, for any chosen thickness x of the filter, the equation (1′) can be approximately replaced by

$$\Delta\lambda \cdot \sum_{i=1}^{n} e^{-\mu(\lambda_i)x} f(\lambda_i) = I(x).$$

The approximation will, of course, be the closer the greater n. In order to determine the n unknown quantities $f(\lambda_i)$ one has only to write down n such linear equations corresponding to a set of n different thicknesses $x_k (k = 1, 2, \cdots n)$ of the filter, all of course for the same set of wave lengths. The factor $\Delta\lambda$, common to all terms and to all equations, may as well be dropped or else thrown upon the f's. In that case each $f(\lambda)_i$ will represent the radiant energy contained within the wave length interval ranging from $\lambda_i - \frac{1}{2}\Delta\lambda$ to $\lambda_i + \frac{1}{2}\Delta\lambda$. Thus, and with the abbreviated symbols $\mu(\lambda_i) = \mu_i, f(\lambda_i) = f_i$, and $I(x_k) = I_k$, the set of equations will assume the form

$$e^{-\mu_1 x_k} f_1 + e^{-\mu_2 x_k} f_2 + \cdots + e^{-\mu_n x_k} f_n = I_k,$$

where $k = 1, 2, \cdots n$.

The thicknesses x_k need not, of course, form an arithmetical series. Their selection, which in wide limits is free, can be suited to the practical circumstances of the case under consideration. If the filtration data I_k are available only for a few x_k and one wishes to avoid interpolation, the selection will have to be made among these few thicknesses. If a smooth filtration curve has been drawn through the discrete observations, the choice will be greatly widened. Since the absorption coefficient

μ increases very rapidly with the wave length, the coefficients of the f_i's will rapidly decrease with increasing suffix i. Thus, in order to give the longer waves contained in a sample of radiation a chance to assert themselves at all in the system of our equations, some at least of the thicknesses must be chosen as small as is feasible. The most important among these is clearly $x=0$ itself, corresponding to the absence of a filter. Let this be x_1. Then $I_1=I(o)$ will stand for the total incident intensity. The value of x_2 will be taken as small as possible and the remaining thicknesses increasingly greater. The particular choice $x_3=2x_2$, $x_4=3x_2$, etc., which offers certain computational advantages, will be considered in the sequel.

The system of n linear equations for as many "ordinates" $f(\lambda)$ of the spectral curve will now become

$$\left.\begin{aligned} &f_1+f_2+\cdots+f_n=I_1\\ &\epsilon^{-\mu_1 x_2}f_1+\epsilon^{-\mu_2 x_2}f_2+\cdots+\epsilon^{-\mu_n x_2}f_n=I_2\\ &\cdots\cdots\cdots\cdots\cdots\cdots\\ &\cdots\cdots\cdots\cdots\cdots\cdots\\ &\epsilon^{-\mu_1 x_n}f_1+\epsilon^{-\mu_2 x_n}f_2+\cdots+\epsilon^{-\mu_n x_n}f_n=I_n \end{aligned}\right\} \tag{3}$$

The problem is thus reduced to solving these equations. If D is the determinant of the system and D_{ik} its minors, the required spectral ordinates will be

$$f_i=\frac{1}{D}\{D_{i1}I_1+D_{i2}I_2+\cdots D_{in}I_n\}, \tag{4}$$

$i=1, 2, \cdots n$. Using the now generally adopted convention, that a term in which a suffix occurs twice is to be summed over all values of the suffix, this solution can be written more concisely

$$f_i=\frac{1}{D}D_{ik}I_k. \tag{4'}$$

With regard to the technicalities of computation, I find the method of determinants the most advisable to adopt, though on several occasions I have used with advantage successive elimination. Even in the latter case, however, one will do well to leave the I_k free. Then the set of final formulae, with numerical coefficients once computed, will serve for the analysis of any x-ray radiation for which the filtration data I_k corresponding to the chosen set of thicknesses of the given filter are available, provided the λ-interval has been made ample enough. The calculation

is somewhat simplified by the circumstance that all the elements of the determinant D are exponentials, so that the resulting terms of D, and of any D_{ik}, will be found by simply adding the exponents (and looking up a log table once only for each term). Using the abbreviation $e^{-\mu_i x_k} = (\mu_i x_k) = (ik)$, the determinant may conveniently be written

$$D = \begin{vmatrix} 1 & 1 & 1 & 1 \\ (12) & (22) & (32) \cdots & (n2) \\ (13) & (23) & (33) \cdots & (n3) \\ \cdots & \cdots & \cdots & \cdots \\ \cdots & \cdots & \cdots & \cdots \\ (1n) & (2n) & (3n) \cdots & (nn) \end{vmatrix}. \tag{5}$$

The term corresponding, e.g., to the diagonal elements will be $(22+33+\cdots+nn)$, and so on. An array such as (5), with the actual numerical values of the "ik", placed at the top of the calculation sheet will serve for the whole procedure. Some of the elements (ik), being relatively small, will drop out effectively, thus simplifying the calculation. This means, however, of reducing the labor will be used with discrimination.

Provided one does not wish to exceed $n=4$ or 5, the procedure will by no means be found too laborious. As a matter of fact, even three "ordinates" give a fairly good idea of the quality of an x-ray radiation.

Before proceeding to numerical examples it may be well to mention here the particular case in which, with $x_1=0$, as before, and any x_2, the remaining thicknesses are consecutive multiples of x_2, i.e.

$$x_3 = 2x_2, \quad x_4 = 3x_2, \quad x_5 = 4x_2, \quad \text{etc.}$$

The advantage offered by such a selection of thicknesses is that it considerably simplifies the form of the determinant and of its minors. In fact, write for brevity $(\mu_1 x_2) = a$, $(\mu_2 x_2) = b$, etc., i.e.

$$a = e^{-\mu_1 x_2}, \quad b = e^{-\mu_2 x_2}, \quad c = e^{-\mu_3 x_2}, \quad \text{etc.} \tag{6}$$

Then

$$D = \begin{vmatrix} 1 & 1 & 1 \cdots \\ a & b & c \cdots \\ a^2 & b^2 & c^2 \cdots \\ a^3 & b^3 & c^3 \cdots \\ \cdots & \cdots & \cdots \end{vmatrix}.$$

This is Cauchy's determinant, which is equal to the product of the differences $a-b$, $a-c$, $\cdots$ $b-c$, etc., and the form of its minors is correspondingly simplified. It will be enough to write here down the complete formulae for the case of $n=3$ and to indicate some of them for $n=5$.

Thus, for $n=3$ and the thicknesses $x_1=0$, x_2, $x_3=2x_2$ the determinant becomes

$$D=\begin{vmatrix} 1 & 1 & 1 \\ a & b & c \\ a^2 & b^2 & c^2 \end{vmatrix} = (a-b)(b-c)(c-a),$$

and its nine minors are

$$\begin{aligned} &D_{11} = -bc(b-c), && D_{21} = -ca(c-a), && D_{31} = -ab(a-b) \\ &D_{12} = b^2-c^2, && D_{22} = c^2-a^2, && D_{32} = a^2-b^2 \\ &D_{13} = c-b, && D_{23} = a-c, && D_{33} = b-a. \end{aligned}$$

Hence the expressions for the three spectral ordinates assume, by (4), the simple form

$$\left.\begin{aligned} f_1 &= \frac{c-b}{D}\{bcI_1-(b+c)I_2+I_3\} \\ f_2 &= \frac{a-c}{D}\{caI_1-(c+a)I_2+I_3\} \\ f_3 &= \frac{b-a}{D}\{abI_1-(a+b)I_2+I_3\} \end{aligned}\right\} \qquad (7)$$

where $D=(a-b)(b-c)(c-a)$. These formulae hold for all cases in which $x_3=2x_2$ and, of course, for any selection of λ_1, λ_2, λ_3.

For $n=5$, with a, b, c, d, e, defined as in (6), the determinant is

$$D=(a-b)\cdots(a-e)\cdot(b-c)(b-d)(b-e)\cdot(c-d)(c-e)\cdot(d-e),$$

and the minors of the fifth row,

$$D_{15}=(b-c)(b-d)(b-e)(c-d)(c-e)(d-e),$$

whence $-D_{25}$, $+D_{35}$, etc. on replacing b, c, d, e by a, c, d, e, etc. Equally simple are the minors of the first row,

$$D_{11}=bcdeD_{15}, \quad D_{21}=acdeD_{25}, \quad \text{etc.},$$

while those of the remaining three rows are somewhat more complicated, namely,

$$D_{12} = -[bc(d+e) + de(b+c)]D_{15},$$
$$D_{13} = [be + cd + (b+e)(c+d)]D_{15},$$
$$D_{14} = -[b+c+d+e]D_{15},$$

but still simple enough for computation.

In order to illustrate the proposed method let us consider the radiation emitted at various potentials by two x-ray tubes (Metalix and Media) for which transmission data with aluminium as filter have been determined by Neeff.[6]

Aiming at three spectral ordinates, let us take the set of thicknesses

$$x_1 = 0, \quad x_2 = 0.1, \quad x_3 = 0.2 \text{ cm.},$$

so that the formulae (7) will be directly applicable. To cover a total interval from 0.1 to 1.3A, which will be ample enough even for the hardest of these radiation samples, let us take the set of wave lengths

$$\lambda_1 = 0.3 \quad \lambda_2 = 0.7 \quad \lambda_3 = 1.1.$$

The corresponding mass-absorption coefficients of aluminium are[7]

$$0.531 \quad 5.00 \quad 20.00,$$

whence, with 2.70 as the density of aluminium, the linear absorption coefficients factorized for convenience by $M = \text{Log } e$,

$$M\mu_1 = 0.623 \quad M\mu_2 = 5.86 \quad M\mu_3 = 23.50 \text{ cm}^{-1},$$

and $a = 10^{-M\mu_1 x_2}$, etc., as in (6), i.e.

$$a = 0.866_3 \quad b = 0.259_4 \quad c = 0.0045.$$

Thus the formulae (7) become

$$\left\{ \begin{array}{l} f_1 = 0.0022I_1 - 0.505I_2 + 1.912I_3 \\ f_2 = -0.0252I_1 + 5.630I_2 - 6.465I_3 \\ f_3 = 1.023I_1 - 5.125I_2 + 4.553I_3. \end{array} \right\} \qquad (7a)$$

Notice by the way the intermittency of signs, which repeats itself in all cases. This set of formulae is ready for the analysis of any x-ray radiation for which the original total intensity and those transmitted through 1 mm. and 2 mm. of aluminium have been measured.

The filtration data for the radiation emitted by the *Metalix* tube at four different potentials[8] are, with $I_1 = I(o)$ as unit intensity,

[6] Neeff, T. C.: cf. Fortschritte a. d. Geb. d. Röntgenstrahlen, *XLI*, 414, 1930.

[7] Table in A. H. Compton's '*X-rays and Electrons*,' 1926, p. 189.

[8] The figures quoted give in each case the maximum potential. Similarly for the Media tube treated below. Cf. Neeff, loc. cit.

	I_2	I_3
at 30 KV	0.0624	0.0210
" 50 "	.0868	.0339
" 70 "	$.121_6$	.0590
" 100 "	$.179_7$	.0931

Substituting these values of I_2, I_3, and $I_1=1$ into (7*a*) one finds the results, $f_i=f(\lambda_i)$, collected in the following table. In its last column the quantum limits, as determined by (2) are inserted.

$f(\lambda)$ for Metalix

KV \ λ	0.3	0.7	1.1	λ_m
30	.011	.190	.799	0.41
50	.023	.244	.733	0.25
70	.054	.278	.668	0.18
100	.089	.385	.526	0.12

Since we have made $I_1=1$, so that also $\Sigma f=1$, each f_i gives directly the fraction of the whole energy (intensity) comtained within the corresponding interval. The first interval extends from 0.1 to 0.5A and contains, therefore, in each case the quantum limit λ_m of the spectrum. The fraction f_1 of energy is then actually to be localized, more stringently, between λ_m and 0.5A., while f_2, f_3 require no such qualification (except that some small part of f_3 may actually be spread beyond 1.3A). Thus, at 70 KV, for instance, 5 percent of the energy is contained between 0.18 and 0.5, 28% between 0.5 and 0.9, and 67% is spread between 0.9 and 1.3A (and possibly beyond). The whole set of results seems to be quite satisfactory, showing a steady shifting of the energy from the longer to the shorter waves, in other words, a progressive "hardening" of the radiation with increasing voltage, in accordance with one's expectations. The figures of the $f(0.3)$ column are also fully consistent with the quantum limits.

As a second example let us take the radiation of the *Media*. The filtrated intensities for this tube, again for 1 and 2 mm of aluminium and with $I_1=1$, are:

	I_2	I_3
at 30 KV	0.128_0	0.0532
" 50 "	0.211_0	.0958
" 70 "	0.296_9	$.157_1$
" 100 "	0.362_3	$.225_5$

Substituting these values in (7*a*), one finds the following spectral composition of the four samples of radiation.

$f(\lambda)$ for Media

KV \ λ	0.3	0.7	1.1
30	.040	.350	.610
50	.079	.542	.379
70	.153	.629	.218
100	.251	.554	.195

This is again a thoroughly consistent and regular set of results. With increasing voltage the intensity of the longest waves is steadily weakened and the shortest waves gain gradually in strength, while the energy contained within the middle λ-interval increases up to a maximum and then, in the neighbourhood of 70 KV, begins to fall off. The quantum limits λ_m of the spectra are as before and harmonize well with the column of the $f(0.3)$-values. From a comparison with the preceding table it would follow that the radiation from Media is, at each potential, considerably harder than that from Metalix. Unlike Metalix, whose four spectral "curves" were all steadily rising and thus could have maxima only at or about 1.1A, only the first spectrum for Media shows this behaviour, and the remaining three indicate the presence of a prominent maximum in the neighborhood of 0.7A.

These two sets of results are such as to inspire sufficient confidence in the Al, 3-analyzer[9] embodied in (7*a*), which ought, therefore, to be reliably applicable to any other specimens of x-ray radiation. (A fixed

[9] A brief reference name of the analyzing set of formulae for *three* wave lengths with Al as filter.

choice of the λ_i being agreed upon, the 'quality' of a radiation would then be characterized by three numbers, such as 0.15, 0.63, 0.22 for Media at 70 KV.)

A similar Cu, 3-analyzer, constructed on the pattern of formulae (7) for the same triad of λ's and thicknesses $x_1=0$, $x_2=.005$, $x_3=.01$ cm, and applied to seven copper-filtration curves corresponding to various potentials, obtained by L. S. Taylor,[10] has also given reasonable results for the spectral energy distribution, but aluminium as analyzing substance turned out to be by far preferable to copper. The latter leads to much greater coefficients in the final formulae and puts thus a higher claim on the accuracy of the I_k-measurements. (Vide infra.)

Passing to higher values of n, several Al,4 and Al,5-analyzers, based on the general formulae (4) with D as in (5), for various sets of λ_i and x_k, were constructed and applied to the radiations of Media and Metalix. For the sake of further illustration of the method it will be enough to quote here in some detail one such example, for $n=4$.

Thicknesses of Al:

$$x_1 = 0 \quad x_2 = .05 \quad x_3 = .10 \quad x_4 = .20 \text{ cm},$$

wave lengths selected:

$$\lambda_1 = 0.3 \quad \lambda_2 = 0.6 \quad \lambda_3 = 0.9 \quad \lambda_4 = 1.2,$$

representing the intervals 0.15 to 0.45, etc. Corresponding $M\mu_i$-values

$$0.623 \quad 3.73 \quad 12.1 \quad 29.7 \text{ cm}^{-1}.$$

Whence the determinant D and its minors D_{ik}. The substitution of these in (4) gives the required formulae,

$$\text{(Al, 4)} \left\{ \begin{array}{l} f_1 = -0.015I_1 + 0.545I_2 - 2.135I_3 + 3.159I_4 \\ f_2 = 0.071I_1 - 2.477I_2 + 9.310I_3 - 7.782I_4 \\ f_3 = -0.295I_1 + 9.495I_2 - 17.76I_3 + 9.115I_4 \\ f_4 = 1.240I_1 - 7.563I_2 + 10.59I_3 - 4.495I_4 \end{array} \right\} \quad (8)$$

Notice, in comparison with (7*a*), the greater values of the coefficients. This increases the effect of the inaccuracies of the observed I_k upon f_i (a circumstance which becomes more serious in the case of $n=5$ when it seems impossible to push some of the coefficients below 50 or 60).

The data for Media, with $I_1=1$, are

[10] Radiology, *XVI*, 302, March, 1931.

	I_2 ($\frac{1}{2}$ mm)	I_3 (1 mm)	I_4 (2 mm)
at 30 KV	0.244_6	0.128_0	0.0532
" 50 "	$.366_2$	$.211_0$	.0958
" 70 "	$.470_5$	$.296_9$	$.157_1$
" 100 "	$.512_1$	$.362_3$	$.225_5$

The substitution in (8) gives the following spectral distribution of intensity

$f(\lambda)$ for Media

KV \ λ	0.3	0.6	0.9	1.2
30	.013	.242	.241	.504
50	.037	.381	.310	.272
70	.105	.444	.333	.118
100	.202	.420	.190	.188

This shows again a marked progressive shift of energy, with increasing potential, towards shorter waves. There is a rather unexpected increase of $f(1.2)$ in passing from 70 to 100 KV, though the last distribution "curve" itself is by no means unlikely. Apart from this and other minor details, the table corroborates substantially the composition found for these radiations before by the Al,3-analyzer. The latter scheme, however, would seem the more advisable to adopt, especially for technical applications.

Let us still estimate the probable error of the f_i obtainable by the proposed method, say for the case of $n=3$, formula (7*a*). Let any one of these formulae be written briefly

$$f = c_1 I_1 + c_2 I_2 + c_3 I_3.$$

Let us take the absorption coefficients and the thicknesses, and therefore the c-values for granted, let δI_2, δI_3 be the probable errors of the filtration data[11] and δf that of f. Then

$$(\delta f)^2 = (c_2 \delta I_2)^2 + (c_3 \delta I_3)^2.$$

[11] Since $I_1 = 1$ rigidly, by convention, $\delta I_1 = 0$.

A moderate estimate of the P.E. of the filtration data is 1 percent of the observed value. Thus

$$\delta f = \pm \frac{1}{100}\sqrt{(c_2 I_2)^2 + (c_3 I_3)^2}.$$

It will suffice to evaluate the greatest of these P.E., which by (7a) is clearly that of f_2 at 100 KV. Inserting the coefficients c_2, c_3 from (7a) and $I_2 = 0.180$, $I_3 = 0.093$, for Metalix, one finds

$$\delta f_2 = \pm\ 0.012, \text{ so that } f_2 = 0.385 \pm .012.$$

Similarly for Media at 100 KV ($I_2 = 0.362$, $I_3 = 0.226$),

$$\delta f_2 = \pm\ 0.025, \text{ and } f_2 = 0.554 \pm .025.$$

These then are the greatest P.E.[12] in the three-ordinate tables for Metalix and Media; the δf_3 are a little smaller and δf_1 considerably smaller. The reader will have no difficulty in calculating the P.E. of the 12 items of each of these tables. Suffice it to say that they are all small enough to make the three-λ method of analysis thoroughly practicable.

For $n = 4$, as in (8), where the coefficients mount almost to 18, the probable errors, especially of f_3, are somewhat greater, but still not serious, while for $n = 5$, when some of the coefficients rise unavoidably higher,[13] these errors δf, due to the δI_k, may become intolerably large, outweighing perhaps the increase of accuracy due to a closer approximation of the integral by a sum of five (instead of three) terms. It is, therefore, not advisable to push the method beyond $n = 4$, unless more accurate filtration data ($\delta I_k / I_k < 1/100$) can be procured.

The proposed method could be applied also to the analysis of samples of visible light by means of appropriate filters for which the absorption coefficient μ as function of λ is available.

In a recent paper by H. Th. Meyer[14] the final form adopted for expressing transmission measurements on x-rays consists in plotting the half-value layers against the thickness of the pre-filter. This has suggested the following slight modification of the above method of spectral analysis of x-ray radiation.

The radiation from a tube having been filtered through a layer of aluminium, say, of any given thickness x, let y be the additional thick-

[12] So far as dependent on the δI_k only.

[13] In none of a large number of my trials (various selections of sets of x_k and λ_i was the greatest coefficient below 52.

[14] *HWS.-Messungen in Aluminium*, Strahlentherapie, *38*, 329, 1930, et seq. "HWS." = half-value layers.

ness of aluminium which reduces the intensity of the prefiltered radiation to one-half. Then

$$\int e^{-\mu(\lambda)(x+y)} f(\lambda) d\lambda = \tfrac{1}{2} \int e^{-\mu(\lambda)x} f(\lambda) d\lambda$$

or

$$\int e^{-\mu(\lambda)x} [1 - 2e^{-\mu(\lambda)y}] f(\lambda) d\lambda = 0,$$

where x, y is any pair of corresponding thicknesses. (Such pairs precisely are plotted against each other in Dr. Meyer's curves.) This, with with μ a known function of λ and y a known function of x, is a homogeneous integral equation for the unknown spectral composition $f(\lambda)$ of the original radiation, to be supplemented by

$$\int f(\lambda) d\lambda = 1,$$

it the total intensity of that radiation is taken as unity.

The integral is again replaced, approximately, by a sum of n terms corresponding to n equally spaced λ_i. Thus, for any pair x_k, y_k of corresponding values of x, y,

$$\sum_{i=1}^{n} e^{-\mu_i x_k} [1 - 2e^{-\mu_i y_k}] f_i = 0, \tag{9}$$

which is a *homogeneous* linear equation for the f's with coefficients all known. It is then enough to write down $n-1$ such equations, with different pairs x_k, y_k ($k = 1, 2, \cdots n-1$). This system will determine the ratios $f_1 : f_2 \cdots f_n$, and (the common factor $\Delta\lambda$ being again embodied in the f_i) the condition

$$\sum f_i = 1 \tag{10}$$

will give the values of $f_1, f_2, \cdots f_n$ themselves.

I have applied this method, with $n = 4$, to Meyer's measurements. The source of x-rays in Dr. Meyer's experiments was a therapeutic AEG tube of type T III, run at a constant potential, fixed for each set of Al-filtrations. Abundant data, such as are required for (9), are gathered in Fig. 4 of Meyer's paper (p. 335) which contains as many as

[15] "HWS" plotted against "*Vorfilter*" (prefilter).

seventeen $y-x$ curves[15] for radiations emitted by this tube at potentials ranging from 30 up to 190 KV.

Nine of these radiation samples were considered, the required three pairs of x, y being in each case read off one of Meyer's curves. The choice of the four wave lengths λ_i was guided by the value of the quantum limit λ_m corresponding to the given voltage.

To explain the procedure it will be enough to describe here in some detail one of these computations, say for the radiation emitted at 50 KV.

The readings from Meyer's curve for this potential are, in mm.,

$$x_1 = 0 \qquad x_2 = 1.0 \quad x_3 = 2.0$$
$$y_1 = 0.90_5 \quad y_2 = 1.29 \quad y_3 = 1.60.$$

Since $\lambda_m = 0.247$, the set

$$\lambda_1 = 0.3 \quad \lambda_2 = 0.5 \quad \lambda_3 = 0.7 \quad \lambda_4 = 0.9,$$

representing the intervals 0.2 to 0.4A, etc., was chosen. The corresponding absorption coefficients of aluminium, per mm., factorized as before, are

$$(M\mu) \quad 0.0623 \quad 0.224 \quad 0.586 \quad 1.208.$$

With these numerical values the three equations of type (9) become

$$-7.56f_1 - 2.54f_2 + 4.10f_3 + 9.74f_4 = 0$$
$$-5.56f_1 - 0.167f_2 + 1.69f_3 + 0.585f_4 = 0$$
$$-4.43f_1 + 0.442f_2 + 0.519f_3 + 0.0375f_4 = 0.$$

Their solution is

$$f_1:f_2:f_3:f_4 = 1.32:7.56:4.74:1,$$

whence, by (10),

$$f_1 = 0.090, \quad f_2 = .517, \quad f_3 = .325, \quad f_4 = .068.$$

In exactly the same way the remaining cases were treated. The absence or scarcity of energy (f_4) within the highest λ-interval has served as an additional hint for shifting the λ-tetrad for the next higher potential towards shorter waves.

The results obtained in this manner for the spectral energy distribution in the radiation emitted by the said AEG tube at nine different potentials are gathered in the following table. Needless to say, the blanks in this table do not signify gaps in the spectra. The subintervals, e.g.,

in the first row extend up to 0.5, from 0.5 up to 0.7, and so on, filling out continuously the total interval. Similarly for the remaining rows. The half-value layers y_1, y_2, y_3, from Meyer's curves, utilized for this table were those corresponding to the same pre-filtrations, $x_1=0$, $x_2=1$, $x_3=2$ mm.

$f(\lambda_i)$ for *AEG* therapeutic tube, type *T* III

KV	λ_m	λ_i									
		0.1	0.2	0.3	0.4	0.5	0.6	0.7	0.8	0.9	1.0
30	0.41				.025		.456		.519		.000
50	0.25			.090		.517		.325		.068	
70	0.18			.257		.510		.189		.044	
100	0.12		.230		.397		.345		.028		
120	0.10		.306		.396		.263		.035		
140	0.09		.397		.349		.243		.011		
160	0.08		.478		.307		.215		.000		
180	0.07	.299		.404		.249		.048			
190	0.06_5	.327		.406		.235		.032			

The whole set seems very satisfactory, showing throughout a regular and steady intensification, with growing potential, of the shorter waves at the expense of the longer ones. The last-described method will be found to offer certain advantages and can be applied whenever y, x data are available. These, of course, presuppose a drawn out filtration curve in the usual sense of the word, $I=I(x)$, from which they are derived (as was done by Meyer) by a simple graphical process: if x' is the abscissa of a point of the filtration curve whose ordinate is $\frac{1}{2}I(x)$, then $y=x'-x$. The first method has a wider field of application, in so far as it requires only the knowledge of transmissions $I(x)$ for a few discrete thicknesses of the filter. The two methods, of course, are essentially equivalent.

My thanks are due to Mr. R. B. Wilsey for suggesting to me this problem.

November, 1931.

A UNIVERSAL SPECTROMETER FOR THE INFRARED

By A. H. Pfund

[Johns Hopkins University, Baltimore, Md. Received March 12, 1932]

It is generally admitted that spectrometers of the fixed-arm type are most convenient for the study of the infrared. The elegant construction of Wadsworth is employed almost universally to prism spectrometers. Since this design is not directly applicable to wire gratings and, in view of the desirability of a universal fixed-arm spectrometer in which prism, echelette or wire grating may be used, interchangably, the following type of instrument has been developed.

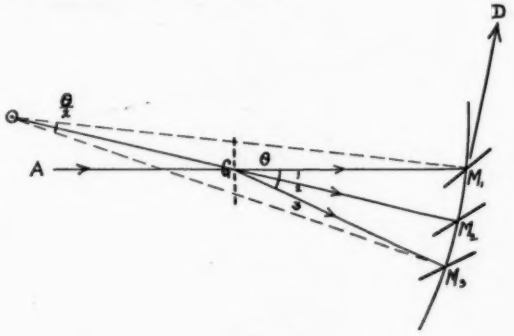

Fig. 1.

The principle underlying this construction may be illustrated by considering the case of the wire grating. If a beam of parallel rays A (Fig. 1) be allowed to fall on a fixed wire grating G and if the desired spectrum range be considered as lying within the angular range of diffraction θ, the several diffracted beams 1, 2, 3 may be given a constant direction D by means of a plane mirror M which, in moving from M_1 to M_3 changes its inclination by the angle $\frac{1}{2}\theta$. This is effected by mounting the mirror on a bar pivoted at O and of such a length that the distance OM_2 is twice GM_2. Briefly, the essential conditions to be fulfilled in this type of construction are:

1. The dispersive device is fixed in position.
2. The actual or apparent point from which the deviated or diffracted beams proceed lies half-way between the pivot O and mirror M_2.
3. The pivot O is so located that the beam of mean deviation lies in the direction OGM_2.
4. The beam of constant direction D lies perpendicular to the direction OM_2.

While the details of construction are omitted it may be pointed out the various parts of the spectrometer are mounted on a substantial

bed-plate of castiron. The dispersive device G is mounted rigidly on a projecting shelf under which the arm OM_2 is free to move. In case of the prism, minimum deviation is established for the sodium lines when the mirror is in the position M_3. This means that for the infrared, which is of smaller deviation, an impairment of spectral purity to due magnification by a prism is avoided. Visual tests, carried out with a Rowland grating of 15,000 lines per inch, have shown that the angle θ may be made as large as 20° without producing more than a barely noticeable lateral shift of the beam D.

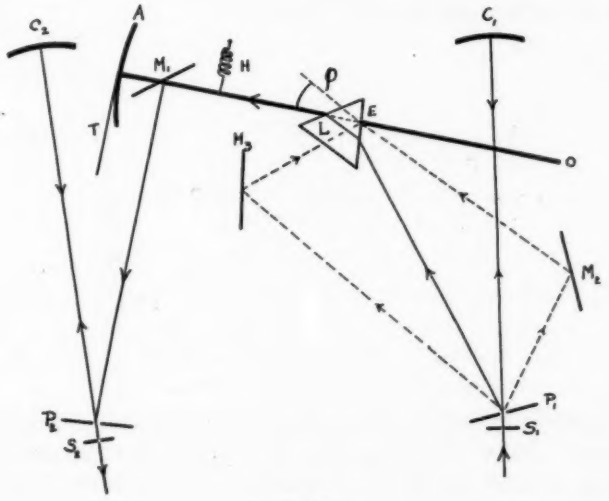

FIG. 2.

In the design of a universal spectrometer it is necessary to combine flexibility and compactness with excellence of optical performance. The preferred design is that involving the use of perforated plane mirrors.[1] These make it possible to use concave mirrors along the optic axis without losing more than 3% of the energy. As shown in Fig. 2, light from the slit S_1 is rendered parallel by the concave mirror C_1 and is returned along the optic axis to the perforated plane mirror P_1 which in turn directs the parallel beam to the prism L (the distance OE being one-half of OM_1). The deviated beam travels parallel to the pivoted arm OM_1 and is reflected from the movable mirror M_1 to the second perforated

[1] A. H. Pfund, J.O.S.A. *4*, 337, 1927.

plane mirror P_2, then, to the concave mirror C_2 which finally, brings the spectrum to a focus in the plane of the exit slit S_2. Beyond this the receiving area of thermopile or radiometer is mounted. The pivoted bar is slotted at M_1 so that the necessary fine adjustment of the position of the mirror M_1 may be made. While the number of reflections employed in this construction is greater than that found in the simpler construction (Fig. 3) the loss of light is not serious—particularly if gold-coated mirrors be used.

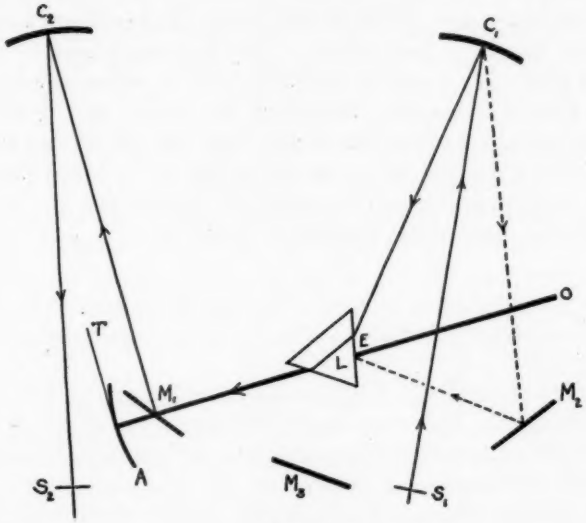

FIG. 3.

The shift of the spectrum across the slit S_2 is effected by means of the usual micrometer screw (not shown) which moves a metal frame guided by "ways." A steel tape T is attached at one end to this frame while the other end is fastened at A to a metallic arc having O at its center. A powerful helical spring H supplies the necessary tension.

In case the prism is to be replaced by a wire grating, the latter is mounted at E and is so oriented as to receive normally the light from an auxiliary plane mirror M_2 which, in turn receives its light from P_1—rotated slightly about a vertical axis to direct the beam to M_2. Since this mirror may be located anywhere between O and P_1 it is readily possible to so direct the beam M_2E that the proper mean angle of diffraction ϕ for any given grating may be realized.

In case the echelette grating is to be used, it is simply mounted so that the ruled surface lies at E. The desired angle of incidence may be realized by sending the light directly from P_1 to M_3 or from M_2 to M_3.

A spectrometer of the above type is under construction. The parabolized mirrors have a focal length of 20 cms and a diameter of 10 cms—thus yielding an aperture of $f2$.

The instrument already constructed is of the simpler design, shown in Fig. 3. Here the mirrors are used off the optic axis. Since the lettering in Fig. 3 corresponds to that in Fig. 2, little need be added to the previous discussion—save, perhaps, that by providing sufficient area on the base-plate, the slit S_1 and mirror C_1 may be moved laterally to make room for mirror M_3 in case the radiation from C_1 is sent directly to M_3.

With properly designed mountings for prism, wire grating and echelette, the change from one to the other may be effected in only a few minutes. Using the same rock-salt prism it was found that in the range of wave lengths extending from 0.6μ to 13μ, the new mounting was quite the equal of the Wadsworth mounting.

ANOMALIES OF VISUAL ACUITY IN RELATION TO STIMULUS-DISTANCE*

By Ellis Freeman

[University of Louisville, Louisville, Kentucky.
Received February 18, 1932]

Some earlier experimental work (1, 2, 3) has revealed an anomaly of visual acuity which is here being investigated further. This anomaly consists of a markedly greater acuity for a large distant constellation than for a small and correspondingly nearer constellation. Obviously this is a violation of the principles of geometrical projection upon which acuity tests, such as the Snellen Charts, are based. For, where the geometrical relationship between distance from the eye and size of stimulus remains constant, together with the intensity of illumination, acuity should theoretically remain constant regardless of variations in the absolute distance and dimensions of the stimulus. But this is precisely what acuity fails to do in such a case. On the contrary a marked difference in acuity occurs, which, until and if an explanation conformable with geometrical optics is found, it is convenient to regard as an anomaly.

This anomaly appears when we employ a specific method of testing, that of gradually separating two bands until they are resolved (minimum separable) as two black lines against an illuminated background, or of gradually increasing the width of an illuminated band until it is distinguished from a black background (minimum visible). Both of these procedures result in greater acuity for the large distant constellation. It is conceivable that this may be only a pseudo-anomaly, arising from uncontrolled dioptrical factors such as accommodation, pupillary width, etc. If these factors were responsible, we should be dealing then with a kind of dioptrical artifact, and not with a proper anomaly, for in such a case the principle of geometrical projection would still serve and require only a simple correction for dioptrics. It is the primary aim of the present investigation to examine the tenability of this latter view.

The observations which originally produced this anomalous phenomenon (1, 2) were made in a well illuminated room with black bands against a large white campimeter. Here pupillary width was not con-

* This work was made possible by a grant from the Howe Fund of the Harvard Medical School, and by the interest and generous assistance of Dr. Frederick H. Verhoeff, Professor of Ophthalmic Research. It was carried out in the Howe Laboratory.

trolled, and the Subject was always aware whether he was regarding a large distant object or a small and correspondingly near one. Furthermore, on account of technical difficulties the work was confined to peripheral vision.

In the investigation reported in this paper central vision only was studied, for the sake of greater theoretical simplicity, and an attempt was made to analyze the conditions under which the anomaly arises, by means of a full control of the following factors:

(1) The awareness of the distance and the apparent magnitude of the stimulus. It was thought that if these "psychological" factors could be eliminated, the anomaly might not appear. Consequently a dark room was employed in which all cues as to distance and size of stimulus were absent. The Subject entered the room in the dark, was allowed a 30 minute period of adaptation, and made all his observations in the dark. Only the Experimenter, who was also one of the two Subjects, knew when he was dealing with the large and when with the small constellation. But as his results paralleled those of the other Subject, the argument against the influence of these "psychological" factors is rendered the stronger. All observations were monocular.

(2) Pupillary width. As decreased accommodation involves increased pupillary width, the higher acuity of the large and more distant constellation might be attributed to a greater flux of light through a wider pupil. To evaluate this factor, an artificial pupil of 1 mm diameter was used in a series of observations.

(3) Accommodation. It is conceivable that as the lens is thinner for the more distant observation of the large constellation, the light rays would apparently be obliged to traverse a thinner layer of lenticular medium, and so suffer less absorption than with the increased accommodation of the small near stimulus. Such a difference in absorption, if great enough, might account for the anomaly. Jaensch (4) has shown in another connection that lenticular thickness is relatively indifferent. However, to evaluate this factor under the conditions of this experiment a glass plate of 2 mm was placed before the eye in one series of observations on the large constellation. It is certain that the interposition of this foreign absorbing layer fully overcame the presumable increase in efficiency of transmission of the thinner lens. If the anomaly were due to the difference in lenticular thickness, it seems reasonable to suppose that the procedure here described would overcome it.[1]

[1] It is conceivable that the crystalline may be effective in favoring the large constellation in still another respect. Perhaps when thin it is a more efficient refracting instrument than

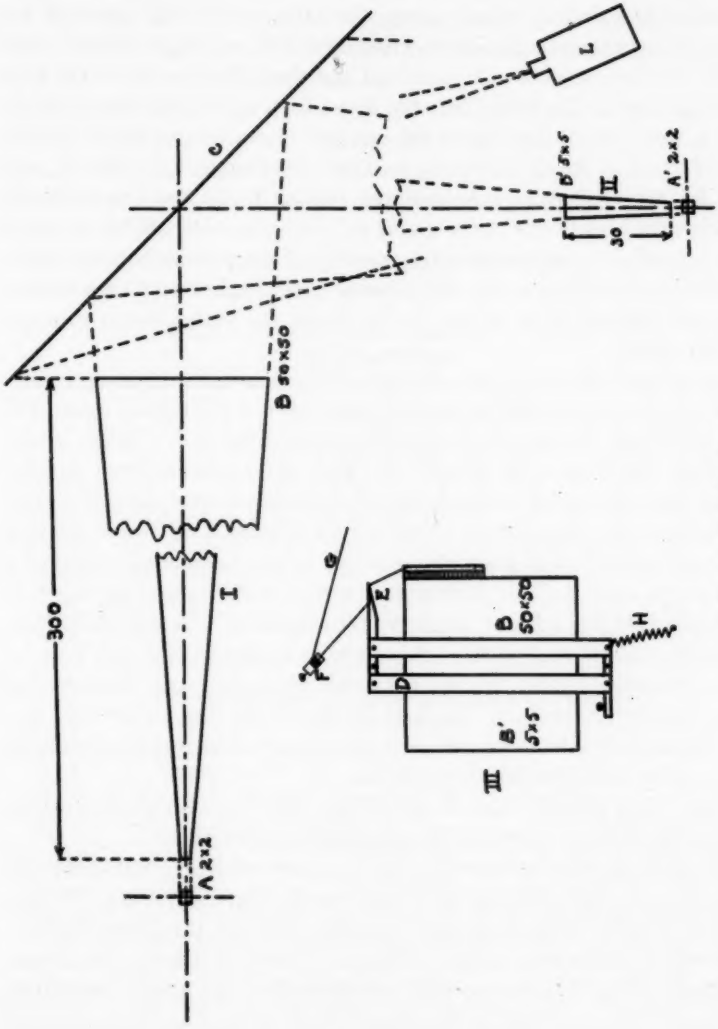

FIG. 1. *The apparatus.*

(4) The retinal gradient. The apparatus is so arranged that the part of the retina corresponding to the dark portions of the figure and field receives no illumination. Consequently the lower limit of the retinal gradient of stimulation may always be taken as *O*. This offers an advantage over the practice of reflecting light from one plane which carries both the dark objects to be resolved and the lighter background. It is obvious that in this latter case the lower limit of the gradient is not *O*, but is equal to the product of the incident intensity and the coefficient of reflection of the dark objects; and that the image of the objects may not be regarded as an unstimulated region. While the precaution of making the lower limit of the gradient *O* is not essential to the study of the anomaly, it does simplify the problem of comprehending the conditions of retinal stimulation, and offers a better opportunity for a mathematical analysis of the acuity curves which the author hopes to make in the future.

Apparatus: The apparatus consists of the arrangement shown in Fig. 1. Part I is a horizontal truncated pyramid of 3 ply veneer wood, 300 cm on its axis, resting at eye-level for a seated Subject. *A* is the ocular opening, 2×2 cm. *B* is 50×50 cm. Part III represents two parallel metal jaws, *D*, each 5 cm wide, placed vertically in the plane of *B*. Observations were begun always with the jaws closed. The cord *G*, passing through pulley *F*, was gradually paid out by the Subject by means of a turn-screw near *A*. This paying out permitted the tension spring *I* to open the jaws the amount necessary for resolution. The pointer *E* indicated on scale *H* the width of this opening to hundredths of a mm.

For determining the minimum visible, two cardboards (not shown) were attached laterally to the jaws *D*, thus darkening all the field but the slit between the jaws, which could be separated until a luminous vertical line could be barely perceived.

Part II is a reproduction of parts I and III, but with all dimensions reduced to 1/10, and is used for the small constellation.

L is a projection lantern used as a source of light, and properly screened from the rest of the apparatus to eliminate stray light. With it a Wratten filter 78AA was used in order to render the illuminant approximately standard daylight in quality. Ground glass screens were interposed in the beam as needed in order to give the desired intensities.

---

when thick; and so, entirely aside from interposing less of an absorbing layer, it may improve acuity by producing clearer images for the large constellation. This possibility would be worth examining, if wholly satisfactory means could be devised.

C is a large vertical surface of stretched white cloth, upon which the light from the lantern is projected. It constitutes the illuminated field against which the jaws of both constellations (wholly unilluminated) are resolved for the minimum separable and the minimum visible. Photometrized by means of a Macbeth photometer, the intensity of *C*, whether from *A* or *A'*, was identical.

Obviously the relation between *I* and *II* is such that for the same intensity of illumination of *C*, we should expect, provided no anomaly existed, the separation of the jaws necessary for resolution in *I* to be tenfold that necessary in *II*. This expectation was, as appears from the data, not fulfilled.

Each value given in the "Slit" column of the tables is the average of four observations made in succession.

TABLE 1. *Minimum separable, under dark-adaptation*
Large constellation

	Subject 1			Subject 2			
Log. *I*	Slit	M.D.	Acuity (1/slit)	Slit	M.D.	Acuity (1/slit)	Average acuity
−3.02855	1.9 mm.	.4	.53	1.9	.3	.53	.53
−3.32098	2.5	.3	.40	2.9	.6	.34	.37
−3.61341	3.2	.3	.31	4.0	1.2	.25	.28
−3.90584	4.5	.7	.22	5.2	0.0	.19	.20
−4.19827	6.8	.7	.15	7.9	.4	.13	.14
−4.49070	8.9	.7	.11	11.7	.6	.09	.10

TABLE 2. *Minimum separable, under dark-adaptation*
Small constellation

	Subject 1			Subject 2			
Log. *I*	Slit	M.D.	Acuity (1/slit×10)	Slit	M.D.	Acuity (1/slit×10)	Average acuity
Same as	.6 mm.	.1	.17	.4	.0	.25	.21
above	.7	.1	.14	.5	.0	.20	.17
	.9	.1	.11	.7	.1	.14	.12
	1.2	.2	.08	1.1	.2	.09	.08
	1.5	.1	.07	1.3	.0	.08	.07
	2.0	.2	.05	1.6	.3	.06	.05

Results: Tables 1 and 2 and Fig. 2 give the acuity results for the minimum separable for two Subjects under dark-adaptation. Taking

either curve alone of Fig. 2, it is apparent that as a function of intensity of illumination acuity varies here in the orthodox manner. But what is unorthodox and anomalous is that the curves for the large and the small constellations do not coincide as they are expected to on the basis of geometrical projection. Rather, at any selected intensity, but particularly the higher intensities used in this work, massive differences in acuity appear, and these are in favor of the large constellation. This disincidence represents the same anomaly already found in the periphery of the light-adapted eye (1, 2). Thus when the Subject works in the dark and is ignorant of the distance and apparent magnitude of the stimulus the same anomaly appears as when he works in the light and is aware of these. Consequently it seems reasonable to suppose that these "psychological" factors are not the cause of the anomaly.

TABLE 3. *Minimum separable, under dark-adaptation, with an artificial pupil of 1 mm diam. Large constellation*

	Subject 1			Subject 2			
Log. *I*	Slit	M.D.	Acuity (1/slit)	Slit	M.D.	Acuity (1/slit)	Average acuity
−2.44369	1.9	.3	.53	1.6	.2	.63	.58
−2.73612	4.3	.3	.23	3.5	.3	.29	.26
−3.02855	5.5	.3	.18	10.5	.3	.10	.14
−3.32098	14.4	1.4	.07				.07

TABLE 4. *Minimum separable, under dark-adaptation, with an artificial pupil of 1 mm diam. Small constellation*

	Subject 1			Subject 2			
Log. *I*	Slit	M.D.	Acuity (1/slit×10)	Slit	M.D.	Acuity (1/slit×10)	Average acuity
Same as above	.5	.0	.20	.4	.0	.25	.22
	1.1	.2	.09	1.0	.2	.10	.09
	1.9	.2	.05	1.6	.2	.06	.05
	2.4	.1	.04				.04

In order to determine the influence of the greater pupillary width which accompanies the large constellation and to which might be attributed its finer acuity, a similar series of observations was made through an artificial pupil of 1 mm diameter placed at the ocular of apparatus *I* and *II*. The results recorded in Tables 3 and 4 show that the

phenomenon still persists. The only difference that arises from the use of the artificial pupil is that acuity has been depressed for the entire range of intensities, and that as a consequence the flux of light at the lower intensities was too small to give any resolution whatever for either constellation, while at the upper end much higher intensities could be employed than were feasible without the pupil. The individual and average acuities of the two Subjects for the small and large constellations show the same characteristic anomaly here as with an uncontrolled natural pupil. If plotted, the two curves would be of the same character as those in Fig. 2, with the one lying considerably above the other. Consequently the anomaly may not be attributed to the differences in pupillary width.

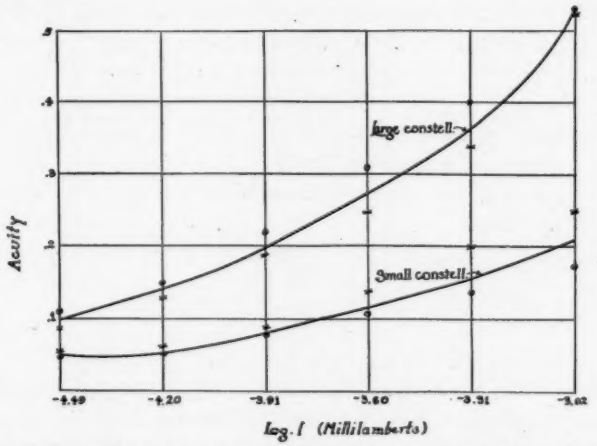

FIG. 2. *Showing disparity in acuity between large and small constellations. Based on Tables 1 and 2. Lines correspond to "average acuity" of both subjects. Circles for subject 1 and crosses for 2 show that there is no overlapping for individuals between the two constellations.*

The next test made bore on the possible influence of differences in lenticular thickness which accompany changes in accommodation. Employing the procedure already described, a transparent glass plate of 2 mm thickness was placed before the eye of one Subject for observations with the large constellation only. This plate probably more than compensated for the thinning of the lens for the large constellation. The resulting slit-widths required for resolution were somewhat increased and the acuity somewhat decreased. Nevertheless, the large constellation still preserved a sufficiently higher acuity curve over the small to give unmistakable evidence of the persistence of the anomaly. It, there-

fore, seems unlikely to suppose that the essential phenomenon arises from differences in lenticular thickness, although it is reasonable to agree that these differences in thickness would tend to influence acuity in the same direction as do the factors which are responsible for the phenomenon.

The lateral cardboards were attached to the jaws, thus leaving only the illuminated slit between them for resolution, and a series of acuities for the minimum visible was determined for both Subjects. Intensities employed were the same as for the minimum separable observations, and as before data was found with and without an artificial pupil. Again the anomaly appeared as for the minimum separable. One expected difference did appear, and that was that the acuity for each constellation of the minimum visible was higher than the acuity of the corresponding constellation of the minimum separable. This is probably due to the circumstance that the minimum visible involves the stimulation of a very small retinal area as compared to the area involved in the minimum separable, so that the maximal dark-adaptation of a relatively larger portion of the retina was preserved.

Subject 2 also made a series of observations under light-adaptation, of both the minimum visible and the minimum separable for each constellation with an uncontrolled pupil. The same anomaly again appeared.

SUMMARY

1. Acuities measured in terms of minimum separable or of minimum visible are greater for a stimulus at 300 cm than for one at 30 cm.

2. This anomalous incongruity may not be attributed to such "psychological" factors as apparent magnitude and awareness of the actual distance of the stimulus; or to differences in pupillary width; or to differences in lenticular thickness which arise from accommodation.

3. As the anomaly occurs with light-adaptation as well as with dark-adaptation it is not a restricted phenomenon.

REFERENCES

1. Ellis Freeman, *Untersuchungen über das indirekte Sehen*, Psychologische Forschung, Bd. *14*, H, 3/4, 332–365, 1931.
2. Ellis Freeman, *Anomalies of peripheral visual acuity*, J. of Experim. Psychol. *12*, 324–340, 1929.
3. Ellis Freeman, *Anomalies of visual acuity in relation to intensity of illumination*, Amer. J. Psychol., *42*, 287–294, 1930.
4. E. R. Jaensch, *Zur Analyse der Gesichtswahrnehmungen*, Z. f. Psychol., Ergänzungsband *4*, 1–140, 1909.

NEW DEVELOPMENTS IN PHOTOELASTICITY

A Purely Optical Method of Stress Analysis

By Arshag G. Solakian

Columbia University, New York, N. Y. Received February 18, 1932]

Introduction

In two dimensional stress problems it is of great importance to determine the directions and magnitudes of the two principal stresses p and q acting at a point in a stressed plate. The various photoelastic methods used in the past in this connection, utilizing polarized light and a transparent isotropic material for the specimen, were more or less a combination of an optical method with a mechanical one. The first method was used to obtain $p-q$, the difference of the two stresses, by measuring the relative retardation of the two refracted rays of a circularly polarized ray of light; the second method was applied to obtain $p+q$, the sum of the two stresses, by measuring the change of thickness of the plate. With $p-c$ and $p+q$ thus known, the values of p and q are easily obtained by an algebraic operation. These two stresses can also be evaluated by means of a "graphical integration" method, developed by Maxwell[1] and later perfected by Filon,[2] through the application of a set of equations for p and q, if the boundary stresses and the directions of the principal stresses and their isoclinics are known.

A purely optical method of determining the magnitudes of the two stresses p and q was first formulated by Neumann[3] in 1841 when he announced the theory of accidental double refraction of a ray of circularly polarized monochromatic light in a strained isotropic transparent media, such as glass. This theory was confirmed later by the experiments of Ernst Mach[4] in 1872 who used a Jamin interferometer in an

[1] C. Maxwell, Scientific Papers, Vol. 1, page 68.

[2] L. N. G. Filon, *On the Graphical Determination of Stresses from Photoelastic Observations*, Engineering, Oct. 19, 1923.

[3] Neumann, "Die Gesetze der Doppelbrechung des Lichtes in comprimierten oder ungleichförmig erwärmten unkrystallinischen Körpern," 1841, Gesammelte Werke, Bd. III, 1912. Teubner, Leipzig.

[4] E. Mach, "Die Doppelbrechung des Glases durch Druck (Optisch-akustische Versuche, Prag, 1873, J. G. Calve'sche Buchhandlung, pages 1 to 25. Also Pogg. Ann., t. CXLVI, p 313; 1872.

investigation of Poisson's ratio, and other physicists, such as W. Voigt,[5] J. Kerr,[6] Pockels,[7] C. Wilson,[8] etc.

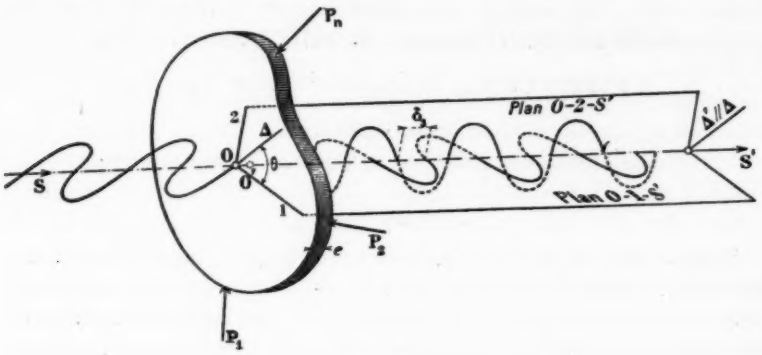

FIG. 1.

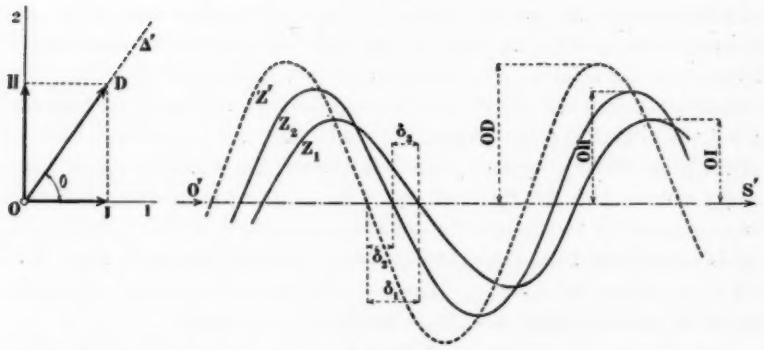

FIG. 2.

DR. H. FAVRE'S METHOD[9]

The method adopted by Dr. H. Favre is based upon Neumann's theory and depends upon the measurements of the absolute phase re-

[5] W. Vogt, Wied. Ann., *15*, p. 497, 1882.

[6] J. Kerr, Phil. Mag., *26*, Oct. 1883.

[7] Fr. Pockels, Bemerkung über das optische Verhalten des comprimierte Glasses, Wied. Ann., *37*, p. 389, 1889.

[8] C. Wilson, "The influence of surface loading on the flexure of beams," Phil. Mag. Series V, vol. XXXII, p. 481–503; 1891.

[9] In preparing this paper, the author has made free abstracts of material and figures, by special authorization, from Dr. H. Favre's thesis on "Sur Une Nouvelle Méthode Optique de Détermination des Tensions Intérieures," published in the Revue Optique Théorique et Instrumentale, Paris, 8 (1929), p. 193–213, 241–261, 289–307.

tardations δ_1 and δ_2 of the two refracted rays, as graphically represented in Figs. 1 and 2, where Z' indicates the ray OS' before the application of the stress and Z_1 and Z_2 the rays $O'S'$ after the application of the stress, and $\overline{OD}$, $\overline{OI}$, $\overline{OII}$ the amplitudes of the two rays respectively.

The time-phase retardations of these rays with respect to the incident ray are given by the equations:

$$\delta_1 = atp + btq, \tag{1}$$

and

$$\delta_2 = btp + atq \tag{2}$$

where a and b are constants depending upon the wave length of the incident ray and the optical and elastic properties of the material used and t the thickness. The relative retardation is then:

$$\delta_1 - \delta_2 = \delta_3 = c(p - q)t \tag{3}$$

where c is equal to $a-b$. The two constants can be determined easily, as will be described later. The values of δ_1 and δ_2 are measured in an optical set for polarized light by means of an interferometer of Jamin, Michelson or Mach-Zehnder type, by observing the movements of the interference fringes during the application of the stress.

A simple proof of the two fundamental equations 1 and 2 for the absolute retardations δ_1 and δ_2 of the refracted rays is as follows:

For a given material and a monochromatic light ray of wave length λ, the values of δ_1 and δ_2 are dependent upon the intensities of the principal stresses p and q, such that:

$$\delta_1 = f_1(p, q) \text{ and } \delta_2 = f_2(p, q);$$

assuming p and q infinitessimally small, develop the functions f_1 and f_2 by Mac-Laurin's series, and neglecting the terms containing powers higher than the second degree, there results:

$$\delta_1 = f_1(p, q) = f_1(0, 0) + \frac{1}{1}\left(\frac{\delta f_1(0, 0)}{\delta p}\, p + \frac{\delta f_1(0, 0)}{\delta q} q\right).$$

When the material is not stressed, it is isotropic and single refracting, hence $\delta_1 = 0$ and $\delta_2 = 0$, in all parts of the material. At the same time $p = q = 0$, so $f_1(0,0) = f_2(0,0) = 0$, therefore,

$$\delta_1 = \frac{\delta f_1(0, 0)}{\delta p}\, p + \frac{\delta f_1(0, 0)}{\delta q} q.$$

By putting $\delta f_1(0,0)/\delta p = a$ and $\delta f_1(0,0)/\delta q = b$, we obtain:

$$\delta_1 = ap + bq.$$

By a similar process, $\delta_2 = bp + aq$.

For a thickness of the material equal to t, the expressions become: $\delta_1 = t(ap+bq)$ and $\delta_2 = t(bp+aq)$, as proposed in eqs. 1 and 2.

It is interesting to observe that the above equations verify Wertheim's law for relative retardation, i.e., $\delta_3 = c(p-q)t$, where c is equal to $a-b$, and $\delta_3 = \delta_1 - \delta_2$.

The formulas derived for δ_1 and δ_2 are also obtained by Dr. Favre, by an entirely different method, based upon Neumann's theory of proportionality between elastic deformation and change in the index of refraction of a given transparent material[10]

Assuming v = velocity of light (monochromatic), n = index of refraction corresponding to the material in its unstressed condition, n_1, n_2 and n_3 the principal indices in the three principal directions of elastic deformations, the following equation can be written, as given by Neumann:[11]

$$n - n_1 = n\left[\frac{\beta}{v}\epsilon_1 + \frac{\alpha}{v}(\epsilon_2 + \epsilon_3)\right] \tag{4}$$

where α and β are the characteristic parameters of the material and light used, and ϵ_1, ϵ_2 and ϵ_3 are the specific linear deformations corresponding to the principal deformations. Similarly:

$$n - n_2 = n\left[\frac{\beta}{v}\epsilon_2 + \frac{\alpha}{v}(\epsilon_3 + \epsilon_1)\right], \tag{4'}$$

and

$$n - n_3 = n\left[\frac{\beta}{v}\epsilon_3 + \frac{\alpha}{v}(\epsilon_1 + \epsilon_2)\right]. \tag{4''}$$

From the theory of elasticity, for a plate in equilibrium, we have

$$\epsilon_1 = \frac{1}{E}\left(p - \frac{q}{m}\right), \quad \epsilon_2 = \frac{1}{E}\left(q - \frac{p}{m}\right) \text{ and } \epsilon_3 = \frac{1}{mE}(p+q),$$

where the direction of ϵ_3 is taken to be normal to the plate.

The optical path of a monochromatic plane polarized light, normally

[10] Bouasse, "Cours de Physique," p. 355 et suiv. 1925. Also Mascart, "Traité d'Optique." Paris, 1891, II. p. 239.

[11] Mascart, "Traité d'optique." Vol. 2, p. 240.

through an isotropic material before the application of the stress, is given by the expression:

$$L = (n - 1)t. \tag{5}$$

After the application of the stress, the original ray refracts into two rays, vibrating respectively parallel to ϵ_1 and ϵ_2. The absolute phase difference of the first refracted ray with regard to the original ray is:

$$\delta_1 = -dL_1 = (n - 1)dt + t \cdot dn. \tag{6}$$

By definition,

$$dt = \epsilon_3 t, \text{ and } dn = n_1 - n = -n\left[\frac{\beta}{v}\epsilon_1 + \frac{\alpha}{v}(\epsilon_2 + \epsilon_3)\right],$$

Hence,

$$\delta_1 = t\frac{1}{E}\left[(n-1)\frac{1}{m} + n\frac{\beta}{v} - 2\frac{n}{m}\frac{\alpha}{v}\right]\cdot p + t\frac{1}{E}\left[(n-1)\frac{1}{m} + \left(1 - \frac{1}{m}\right)n\frac{\alpha}{v} - \frac{n}{m}\frac{\beta}{v}\right]\cdot q.$$

Similarly, ϵ_2, the absolute phase difference of the second refracted ray with respect to the original ray is obtained, by permutation of ϵ_1 and ϵ_2, that is, p and q:

$$\begin{aligned}\delta_2 = t\frac{1}{E}&\left[(n-1)\frac{1}{m} + \left(1 - \frac{1}{m}\right)n\frac{\alpha}{v} - \frac{n}{m}\frac{\beta}{v}\right]p \\ &+ t\frac{1}{E}\left[(n-1)\frac{1}{m} + n\frac{\beta}{v} - 2\frac{n}{m}\frac{\alpha}{v}\right]q.\end{aligned} \tag{7}$$

It is obvious that, δ_1 and δ_2, as given in the eqs. 5 and 7, have the same form as first expressed in the eqs. 1 and 2, that is:

$$\delta_1 = t(ap + bq) \text{ and } \delta_2 = t(bp + aq).$$

On account of the errors of observations during the measurements of δ_1, δ_2 and δ_3, the eqs. 1, 2 and 3 will be written:

$$\left.\begin{aligned}\delta_1 + v_1 &= t(ap + bq)\\ \delta_2 + v_2 &= t(bp + aq),\\ \delta_3 + v_3 &= t(p - q)c,\end{aligned}\right\} \tag{8}$$

where v_1, v_2 and v_3 are the respective errors of observations. Let p_1, p_2 and p_3 to be the " weights" (in the sense attributed by Gauss) of obser-

vations.[12] Consider v_1, v_2 and v_3 as functions of p and q. In these conditions the expression $p_1v_1^2+p_2v_2^2+p_3v_3^2=\sum(pv^2)$ also can be considered as a function of p and q. According to Gauss, the most probable values of p and q are determined by the condition that $\sum(pv^2)$ should be a minimum, or as in the equations

$$\frac{\delta\sum(pv^2)}{\delta p}=0, \quad \frac{\delta\sum(pv^2)}{dq}=0.$$

The most probable values of p and q, and also the mean errors μ_p and μ_q of the results obtained are found by the following equations:

$$\left.\begin{aligned} p &= R_{11}\delta_1+R_{21}\delta_2+R_{31}\delta_3,\\ q &= R_{12}\delta_1+R_{22}\delta_2+R_{32}\delta_3,\end{aligned}\right\} \tag{9}$$

$$\left.\begin{aligned} \mu_p &= \pm\,\theta_1(\delta_1-\delta_2-\delta_3),\\ \mu_q &= \pm\,\theta_2(\delta_1-\delta_2-\delta_3).\end{aligned}\right\} \tag{10}$$

These four equations are of fundamental importance, as they give us directly the values of the principal stresses and their mean errors as functions of the intensities of δ_1, δ_2 and δ_3 determined optically.

The coefficients R_{11}, R_{21}, R_{31}, R_{12}, R_{22}, R_{32}, θ_1 and θ_2 depend upon the coefficients a, b, c, the thickness t of the model, and the weights of observations p_1, p_2, and p_3. These coefficients are constants for a given model and are given in the following expressions:

$$R_{11}=\frac{a\left(\frac{1}{p_1}+\frac{1}{p_3}\right)-b\left(\frac{1}{p_2}\right)}{tc(a+b)\left[\frac{1}{p}\right]}, \quad R_{21}=\frac{a\left(\frac{1}{p_1}\right)-b\left(\frac{1}{p_1}+\frac{1}{p_3}\right)}{tc(a+b)\left[\frac{1}{p}\right]},$$

$$R_{31}=\frac{a\left(\frac{1}{p_1}\right)+b\left(\frac{1}{p_2}\right)}{tc(a+b)\left[\frac{1}{p}\right]},$$

$$R_{12}=\frac{a\left(\frac{1}{p_2}\right)-b\left(\frac{1}{p_2}+\frac{1}{p_3}\right)}{tc(a+b)\left[\frac{1}{p}\right]}, \quad R_{22}=\frac{a\left(\frac{1}{p_1}+\frac{1}{p_3}\right)-b\left(\frac{1}{p_1}\right)}{tc(a+b)\left[\frac{1}{p}\right]},$$

[12] Gauss: Theoria combinationis observationum erroribus minimis obnoxiae, (Gottingae, 1823).

$$R_{32} = \frac{-a\left(\frac{1}{p_2}\right) - b\left(\frac{1}{p_1}\right)}{tc(a+b)\left[\frac{1}{p}\right]}.$$

$$\theta_1 = \frac{\sqrt{p_1b^2 + p_2a^2 + p_3c^2}}{tc(a+b)\left[\frac{1}{p}\right]\sqrt{p_1p_2p_3}}, \qquad \theta_2 = \frac{\sqrt{p_1a^2 + p_2b^2 + p_3c^2}}{tc(a+b)\left[\frac{1}{p}\right]\sqrt{p_1p_2p_3}}.$$

In the above formulas,

$$\left[\frac{1}{p}\right] = \frac{1}{p_1} + \frac{1}{p_2} + \frac{1}{p_3}.$$

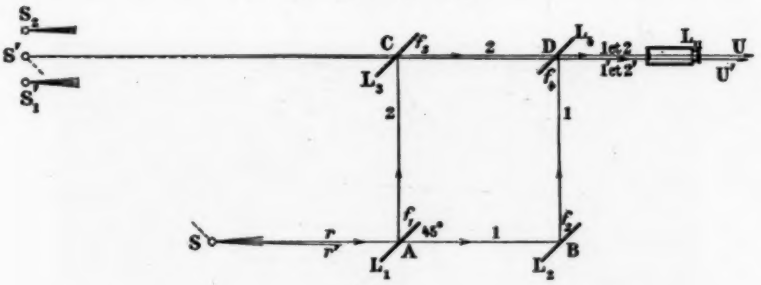

FIG. 3.

It is evident from these equations that the values of p and q stresses can be calculated if the numerical values of δ_1 and δ_2 are known. These are determined by Dr. Favre by means of a Mach-Zehnder type interferometer of four mirrors, in addition to the optical set for polarized light.

The Mach-Zehnder Interferometer.[13] This interferometer possesses the advantage of measuring the phase difference of a ray of circularly polarized light vibrating in a given direction. The essential parts of the instrument are, as shown in Figs. 3, 4 and 5:

(a) Four silvered plates L_1 L_2, L_3 and L_4 located at the corners of a square 330 mm on each side. The rectangular openings for the mirrors are 40×30 mm. The mirror holders are attached to a base plate G having the form of U, which allows the placing of the model in the path of ray 1 in the opening *abcd*. The plates can be rotated through

[13] Zehnder, ZS. für Instrumentenkunde, No. 11, 1891, p. 275. Mach: ZS. für Instr., No. 12, 1892, p. 89, and Wiener Berichte, No. 107, p. 851.

any vertical or horizontal angle by means of a system of screws and levers. Plates L_1 and L_3 are fixed, while L_2 and L_4 can be moved in a direction parallel to the normals to their faces.

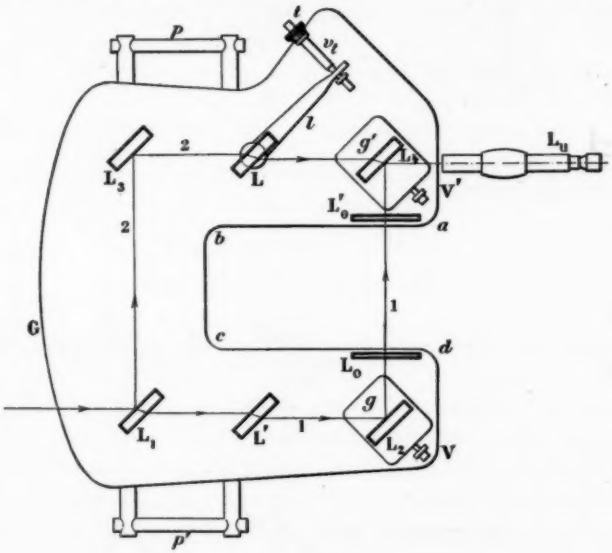

FIG. 4.

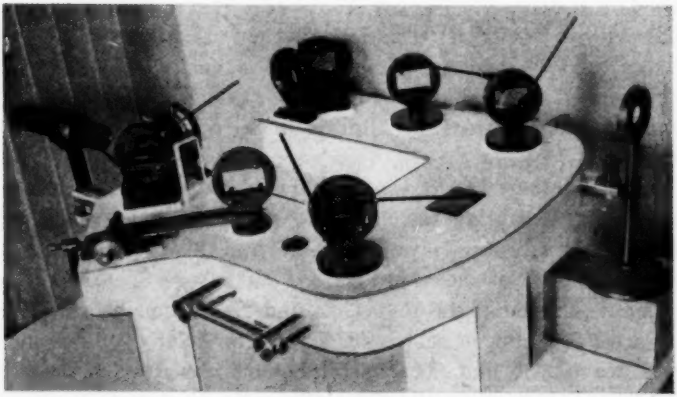

FIG. 5.

(b) A compensator, made of a plate of glass 7 mm thick, with parallel faces, placed in the path of the ray 2 midway between L_3 and L_4. By

means of a micrometer screw attached to the cylinder t, the lever l causes a motion of rotation to the plate L around its vertical axis. By turning the screw v_t the optical path of the ray 2 and the angle between the plate and the ray are changed. Hence, interference fringes will be put into motion. The compensator is calibrated in such a manner that one complete rotation of the barrel corresponds to the displacement of 10 fringes, with the plate L making an angle of 45° with the ray 2.

(c) A glass plate L', 7 mm thick and with parallel faces, placed in the path of the ray 1, midway between L_1 and L_2 and parallel to the other four plates. Its function is to give to ray 1 the same optical path as that of ray 2.

(d) Two half-wave mica plates L_0 and L_0', placed in the path of ray 1, on both sides of the model. Each plate is provided with a gradu-

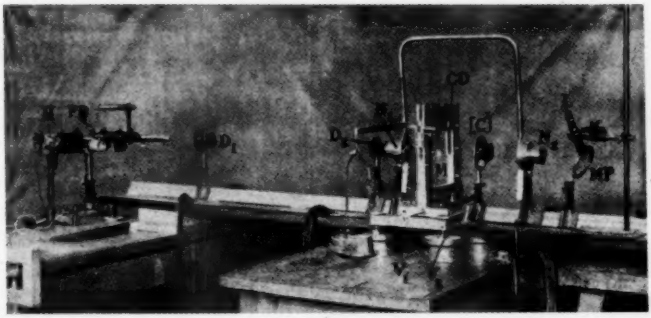

FIG. 6.

ated circular vernier in order to orient its optical axis at a given direction.

(e) A telescope Lu fixed to the holder G, and provided with a set of cross hairs for the observation of the motion of the interference fringes.

Determination of α—In order to measure α, the angle between p and the vertical, the following arrangment of the optical set is used, as shown in Fig. 6. This consists of a mercury lamp H, a prism of constant deviation of Pellin-Broca PB to get parallel rays, two diaphragms D_1 and D_2 with circular holes 10 mm in diameter, two crossed Nicols N_1 and N_2 rigidly connected with each other but free to rotate together around their horizontal axis, another diaphragm with a hole 1 mm in diameter and in line with the axis of the Nicols, the model M in

the loading frame CD in between the two Nicols, a diaphragm of the same size as the model and attached to it, having circular holes 0.5 mm at points where the values of p and q stresses are to be determined, a plane mirror MP next to the analyzer N_2 with the normal to the mirror making an angle of 45° with the ray, and finally, a telescope to receive the reflected ray by the mirror.

When the model is stressed, a luminous spot will appear in the telescope when one of the holes of the diaphragm is in line with the path of the incident rays. If now we rotate the crossed Nicols until this brilliant spot darkens completely, at this point the principal sections of the Nicols are respectively parallel to the two principal stresses acting at the point in the model. The reading on the graduated circular vernier attached to the analyzer N_2 will give the value of the angle α. The accuracy of observations for α lies within 15′.

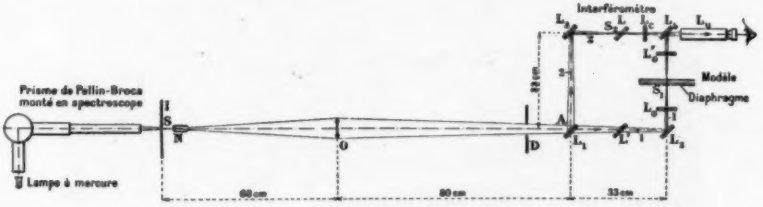

FIG. 7.

Determination of δ_1 *and* δ_2—In Fig. 7 the mirror plates are represented by L_1, L_2, L_3 and L_4. In I is placed a diaphragm having a hole at s 0.2 mm in diameter, through which travels the green light of 5461A wave length obtained from a mercury vapour lamp and a Pellin-Broca prism. On the right SA successively are placed starting from S, a Nicol prism N, a lens L and a diaphragm D with a circular hole of 18 mm in diameter. The ray 1 gives a real image of S at S_1, and the ray 2 a real image of the same source at S_2. The lens O is placed in such a manner that S_1 is madway between the two plates L_2 and L_4. The ray has a diameter of about 0.4 mm at S_1 and thus it can easily pass through the hole of the diaphragm placed in front of the model.

In order to compensate for the thickness of the model which affects the optical path of the ray 1, a plate L_c of the same material and thickness as the model, is placed in the path of the ray 2.

The ray SA is polarized during its passage through the Nicol N and vibrates in a vertical plane, coinciding with the principal section of the

prism. The rays 1 and 2 are also polarized and have their vibrations in a vertical plane. After leaving the interferometer, the two rays may interfere.

In order to have the ray 1 vibrate parallel to one of the principal stresses acting at a point through which the ray passes out of the model, the optical axis of the half-wave mica plate L_0 is oriented properly by means of the graduated circle. The verticality of the vibrations of the ray 1 after its passage through the model, is established by orienting properly the optical axis of the second half-wave mica plate L_0'.

The process of determining δ_1 for a given point is as follows:

(a) Place the diaphragm with its opening corresponding to the point in question, in line with the ray 1.

(b) Orient the axes of the half-wave plates. Supposing at a point the angle α between the p stress and the vertical to be $+30°$, the optical axis of the half-wave plate L_0 is turned through $+15°$ from a vertical. The vertical plane of vibrations of the ray 1 is thus turned through 30° and coincides with the direction of p stress. In order to reestablish the verticality of the plane of vibrations after leaving the model, it is necessary to incline by $+15°$ the perpendicular to the optical axis of the second half-wave plate.

(c) Observe through the telescope before applying the load. By turning the screw v_t, the fringes are put into motion until one of them is symmetrically placed between the two vertical cross hairs. The reading on the circle t is recorded. During the application of the load the fringes are displaced, because the optical path of the ray 1 is varied by δ_1. Now bring back in between the two cross hairs the fringe which was seen originally. Take the reading of the second position of the circle. The difference between the two readings will give the value of δ_1, the circle being calibrated in terms of wave lengths. The approximation is in 3/100 of a wave length.

δ_2 is measured by a similar process.

Thus having the values of δ_1 and δ_2, the corresponding values of p and q stresses are computed from eqs. 1 and 2, if the values of the constants a and b are also known for the given conditions of material, source of light, etc.

Determination of the constants a, b, and c. These are found by measuring δ_1, δ_2 and δ_3 at a point in a model where the values of the principal stresses are known. Consider for example the prism of glass of which the dimensions are H, h and t, as shown in Fig. 8 and is acted upon by

the two colinear equal and opposite compressive forces V, along its longer axis. Provided the value of H is at least five times larger than either values of h or t, the values of the principal stresses at O are, as shown on the right of the figure, $p=-V/th$ and $q=0$. The values of δ_1, δ_2 and δ_3 at a point O are determined by bringing the $H\times h$ face of the model in the parallel path of the rays. The system of the eqs. 1, 2 and 3 reduce in this case to the following simple ones:

$\delta_1=atp$, $\delta_2=btp$ and $\delta_3=ctp$, from which the values of a, b and c are found to be:

$$a=\delta_1/tp, \quad b=\delta_2/tp \quad \text{and} \quad c=\delta_3/tp.$$

For a prism of glass made by Zeiss (Optisches Gussglas B.K.7) of $10\times10\times60$ mm, Dr. H. Favre has found the following results (corrected for the most probable values by the method of least squares):

$$a=+0.03601\pm0.00014\lambda, \quad b=+0.08530\pm0.00014\lambda,$$
$$c=-0.04929\pm0.00003\lambda.$$

It is interesting to observe that the value of $c=a-b$ is within an error of 0.6 percent.

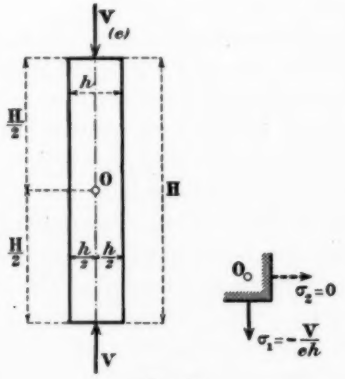

FIG. 8.

The mean errors of observations for δ_1, δ_2 and δ_3 are:

$$\mu\delta_1=\pm0.0282\lambda, \quad \mu\delta_2=\pm0.0282\lambda \text{ and } \mu\delta_3=\pm0.0030\lambda.$$

Determination of $\delta_1-\delta_2=\delta_3$. As an independent check on the accuracy of δ_1 and δ_2 as determined above separately, the value of $\delta_1-\delta_2=\delta_3$ is determined by introducing a compensator of Bravais (Soleil-

Babinet) in the optical set. The essential parts of the compensator, as shown in Fig. 9 are as follows:

Three quartz plates designated by L_1, L_2 and L_3. The plate L_1 has two parallel faces and its optical axis is along Ox. The plates L_2 and L_3 are wedges of quartz with equal wedge angles and with their axes along Oz. A monochromatic ray of circularly polarized light vibrating parallel to Δ, during its passage through L_1 will be decomposed into two rays, vibrating parallel to O_x and O_z, with a phase retardation $\delta' = k\overline{OA}$. The resultant retardation is therefore $\delta = \delta' - \delta'' = k(\overline{OA} - \overline{O'A'})$. When $\overline{OA} = \overline{O'A'}$, then $\delta = 0$.

One of the wedges is fixed, while the other is movable through a system of gears attached to a disk, which is graduated with the divisions

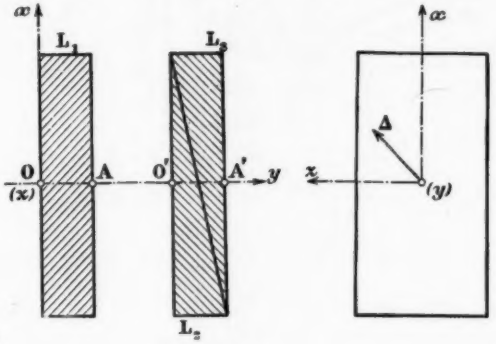

FIG. 9.

proportional to δ. If the two polarized rays, having an initial phase difference δ_3, arrive at the compensator with their vibrations respectively parallel to the axes O_x and O_z, their final phase difference upon leaving the compensator will be $\delta_3 + \delta$. The compensator is mounted on a graduated circle and it is possible to orient the axes O_x and O_z in any desired direction.

In order to measure δ_3, the compensator is placed in between the polarizer and the model, with the axes O_x and O_z parallel to the principal stresses p and q at a given point. The crossed Nicols are oriented with their principal axes at 45° with the directions of p and q stresses. The circle of the compensator is put at zero. If now we look through the telescope, a brilliant spot will appear due to the phase difference of the refracted rays produced by the stressed model. By rotating the graduated circle attached to the movable wedge, the brightness of the

spot is gradually reduced until extinction of the light is produced. At this position, the retardation δ_3 produced by the model is compensated by the retardation δ produced by the quartz compensator. This means $\delta_3+\delta=O$. The reading of the circle is then equal to $-\delta_3$ or $\delta_3=\delta_1-\delta_2$. The accuracy of the Bravais compensator has been found to be within 3/1000 of a wave length.

Illustrative Problem—In order to give an idea of the degree of precision of Dr. H. Favre's optical method of stress investigation, Fig. 10

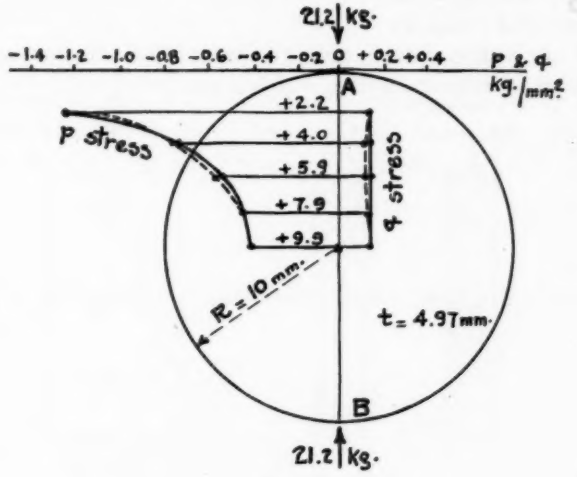

FIG. 10.

is reproduced here, giving the results obtained by Dr. H. Favre in the experiment of a circular disk of Zeiss glass, 20 mm diameter and 4.97 mm thick, compressed by two equal and opposite forces of 21.2 kgs each acting at the extremeties of the diameter AB. The dotted curve represents the variation along AB of the intensities of the two principal stresses p and q determined optically. The p stress is in the direction of AB, while the q stress perpendicular to it. The curve in full line is obtained theoretically.[14] The agreement between the two curves is very close, thus showing the accuracy of the method proposed by Dr. H. Favre and the precision of the apparatus.[15]

[14] Pigeaud, "Résistance des Materiaux et Elasticité, 1920, p. 718, Paris.

[15] The photoelastic apparatus of the "Laboratoire de Photoélasticité de l'Ecole Polytechnique Fédérale de Zurich," of which a description is given in this paper, was designed by Dr. H. Favre and built by the firm Schiltknecht, Zurick.